May 15, 2015

SiD Linear Collider Detector R&D
DOE Final Report

Steering Group: J. Brau (co-PI), M. Breidenbach, M. Demarteau (co-PI),
J. Jaros, H. Weerts, A. White

This report presents a summary of the results of the SiD university detector R&D projects supported by DOE in FY10, FY11, and FY12 with no-cost extensions through February, 2015.

SiD has been designed to address fundamental questions of particle physics:

- What is the mechanism responsible for electroweak symmetry breaking and the generation of mass?
- How do the forces unify?
- Does the structure of space-time at small distances show evidence for extra dimensions?
- What are the connections between the fundamental particles and forces and cosmology?

SiD will address these questions at a next generation linear collider (the International Linear Collider or CLIC) through precision measurements, such as Higgs boson properties, gauge boson scattering, effects resulting from the existence of extra dimensions, properties of supersymmetric particles, and top quark properties. Silicon detectors are used extensively in SiD and are well-matched to the challenges presented by ILC physics and the ILC machine environment. They are fast, robust against machine-induced background, and capable of very fine segmentation. SiD is based on silicon tracking and silicon-tungsten sampling calorimetry, complemented by powerful pixel vertex detection, and outer hadronic calorimetry and muon detection. Radiation hard forward detectors which can be read out pulse by pulse are required. Advanced calorimetry based on a particle flow algorithm (PFA) provides excellent jet energy resolution. The 5 Tesla solenoid is outside the calorimeter to improve energy resolution. PFA calorimetry requires fine granularity for both electromagnetic and hadronic calorimeters, leading naturally to finely segmented silicon-tungsten electromagnetic calorimetry. Since silicon-tungsten calorimetry is expensive, the detector architecture is compact. Precise tracking is achieved with the large magnetic field and high precision silicon microstrips. An ancillary benefit of the large magnetic field is better control of the e^+e^- pair backgrounds, permitting a smaller radius beampipe and improved impact parameter resolution. Finally, SiD is designed with a cost constraint in mind.

The SiD R&D program was designed to establish the new capabilities needed to enable the realization of this innovative detector concept. The SiD design and plan was validated

by the International Detector Advisory Group (IDAG) in 2009, launching a phase of detector development that led to a Detailed Baseline Design (DBD) report, published as one volume of the ILC Technical Design Report in 2013. Many of the technologies needed to enable this powerful detector did not yet exist. R&D was essential to establish them. The projects were conducted by university groups in collaboration with US HEP laboratories and overseas institutions, all working toward realization of these advanced capabilities. A number of the projects resulted in critical results with impacts outside the immediate ILC detector arena.

The set of DOE funded projects includes vertex detector sensor development (4.1), four contributing to the tracker work (5.8, 5.10, 5.22, and 5.23) and five calorimeter projects, four hardware (6.5, 6.6, 6.9, and 6.27) and one on particle flow algorithms (6.4). Following a brief overview on each project below, we attach the final reports. Direct collaboration with national laboratories is indicated just below the title of each project in the overview.

Chronopixel – Oregon/Yale (Project 4.1)

This project developed a vertex sensor meeting the requirements of the ILC, with single bunch crossing time stamping and power constraints. This was achieved in monolithic CMOS working in cooperation with the Sarnoff Corporation in Princeton, NJ.

Alignment – University of Michigan (Project 5.8)

(SLAC)

The frequency scanned laser interferometry alignment project was a critical element in the SiD design. It has significant generic impacts. The very low mass support structures are potentially non-rigid, requiring precision monitoring of changes, such as those caused by temperature changes. ILC detectors will operate in a push-pull arrangement and precise verification of internal stability after movement is essential to achieve the required physics performance.

Silicon Development - UC Santa Cruz (Project 5.10)

(SLAC)

The effort at SCIPP, UCSC, focused on several aspects related to the development of silicon detectors, based on both hardware and simulation studies. The hardware studies included the use of charge division to determine longitudinal coordinates for strip electroides, length limitations for reading out mips, and electromagnetic radiation damage studies. The simulation dealt with non-prompt track reconstruction and the strategy for segmenting the ILC BeamCal.

DC-DC Conversion – Yale (Project 5.22)

This project addressed the fundamental aspect of increasing the efficiency of power delivery for future experiments without adding to the material budget. A study was carried out for the powering of the front-end of the vertex detector readout, focusing on commercially available air core conductors and transformers, working towards an input-output voltage ratio more than ten, with a conversion efficiency exceeding 85%. DC-DC converter plug-in cards with air coils were developed and tested.

Sensors and Connects – University of New Mexico (Project 5.23)

(Fermilab)

To achieve the tight requirements on material budget, the silicon tracker of the SiD detector employs a hybrid-less sensor design. Traces are routed to bump-bonded KPiX chips through a double-metal layer. Signal and control lines run from the KPiX chip to a flex cable, which carries the signals outside of the tracking volume. This project addressed critical issues at the heart of the low-mass tracker design.

Silicon-tungsten EM calorimetry – Oregon/UCDavis (Project 6.5)

(SLAC, BNL)

The goal of this project was to produce a test module using the same technology that would be employed in a collider detector. Innovations in integrated readout electronics, interconnect technologies, and silicon sensors led to development of a dense, highly-segmented electromagnetic sampling calorimeters (ECal) using alternating layers of silicon readout and tungsten radiator. A prototype test version of the calorimeter was tested in beam at SLAC.

GEM-based Digital hadron calorimetry - UT Arlington (Project 6.6)

(SLAC)

To develop digital hadron calorimetry, UTA constructed and tested several 30cm x 30cm double-GEM chambers with anode layers divided into 1cm x 1cm pads. Readout was via the SLAC KPiX chip (64-channel version used so far). Successful operation of these chambers was demonstrated with Fe-55 and Ru-106 sources, and with cosmic rays.

RPC studies – Princeton (Project 6.19)

This R&D project for calorimetry or muon system RPCs investigated the BESIII-type RPC aging phenomena.

RPC-based Digital hadron calorimetry – Boston/Iowa (Project 6.27)

(ANL)

In order to validate the Digital Hadron Calorimeter (DHCAL) concept, gain experience running large Resistive Plate Chamber (RPC) systems and measure hadronic showers in great detail as well as validate the hadronic shower models, a large prototype section of 38 layers and a tail catcher section with 13 layers were constructed. The total readout channel count was close to 470000. The beam test program produced hadronic showers with unprecedented spatial resolution measurements and validated the concept of a digital hadron calorimeter.

SiD Particle Flow Algorithm Development – Iowa (Project 6.4)

(SLAC)

The U. Iowa group (with two members based at CERN), worked to improve the performance of the SiD/Iowa Particle Flow Algorithm. SLAC contributed many basic studies to support algorithm development and is working on a new version of the SiD geometry with more realistic subsystem configurations.

Chronopixel

J. Brau, N. Sinev, D. Strom
Center for High Energy Physics, University of Oregon
.
C. Baltay, W. Emmet, D. Rabinowitz
Yale University

The superconducting design adopted for the ILC (the International Linear Collider) set the parameters required for a vertex detector at the ILC. Based on these requirements we have developed a new concept for vertex detectors based on monolithic CMOS detectors that we call Chronopixels. This concept, developed in collaboration with the SARNOFF silicon fab house, is ideally suited for the ILC application. Our novel new design includes the ability to store the time of each hit in the vertex detector with sufficient accuracy that each hit can be assigned to a unique beam crossing. This will reduce the confusion due to high occupancy to a negligible level.

The Chronopixel project concerns the development of an innovative monolithic CMOS pixel vertex tracker with multi-bunch storage capability. We have explored monolithic CMOS devices where the readout electronics are fabricated on top of an epitaxial layer of silicon that is sensitive to minimum ionizing particles (MIPs). In hadron colliders such devices have the potential to dramatically lower the cost of the upgrades foreseen by the LHC experiments. In lepton colliders, integrated CMOS devices allow pixel-based vertex detectors to be constructed with high resolution and with a small material budget. The 15 μm x 15 μm pixels allow for space point resolution of better than 4 μm commensurate with that of the 3.9 μm resolution that was achieved with the very precise SLD CCD detector[1]. The integrated technique allows for reduction of material over that achieved at SLD to as low as 0.1% X_0. Devices with these parameters would be ideally suited to flavor tagging at a lepton collider and to precise determination of Higgs branching ratios to charm, bottom and taus.

In past years we have tested the first and second prototypes of our design for a monolithic CMOS device that should meet the ILC vertex detector requirements [2], and have potential impact on detectors for other colliders, such as CLIC, e^+e^- circular colliders, the Muon Collider, and, perhaps, even the LHC. This design was developed primarily by the Sarnoff Corporation[3] through R&D contracts, with input from our Yale/Oregon collaboration, particularly by N. Sinev of Oregon. In the ultimate design, each pixel (smaller than 15 μm $\times$15μm) contains electronics to store the bunch number (time) of multiple hits (two or more) above an adjustable threshold (thus the name "Chronopixels"). This capability to assign the hits to individual buckets of the ILC bunch trains is unique to the Chronopixel design. Hits are read out during the 199 msec between bunch trains. The pixels can achieve up to 3 to 4 μm precision without analog information.

The highest hit rates and occupancies result from the estimated 0.03 hits/mm^2/ bunch crossing for the innermost layer, for a bunch train pixel occupancy approaching 10 percent. The time information (i.e., bunch crossing number) reduces this occupancy to $<< 10^{-4}$ per pixel giving considerable headroom should occupancies be higher than expected.

In our second prototype we decided to use low power (see below) NMOS for the in-pixel circuitry in a 90 nm process, retaining CMOS elements for the out-of-pixel interface logic. This has the enormous advantage that the non-standard deep p-well will not be needed and that the only non-standard step needed for the ultimate design would be the 20μm thick epilayer. A second advantage

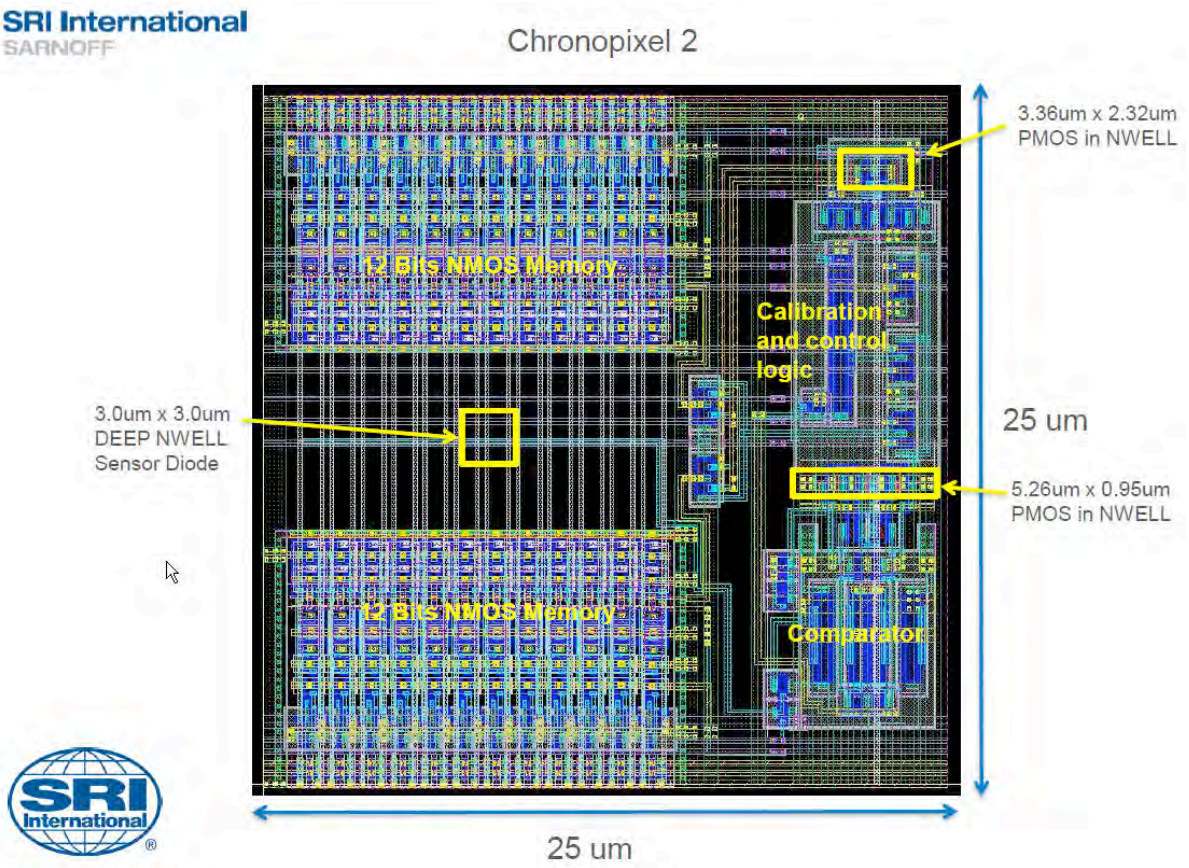

Figure 1: Layout of the second prototype for a $25\,\mu\text{m} \times 25\,\mu\text{m}$ pixel cell.

of using this scheme is that the NMOS transistors can be placed adjacent to each other without the isolation that is required for the complementary PMOS and NMOS transistors used in a CMOS circuit. As a result we can design a pixel with a smaller footprint and we can consider processes with larger feature sizes. This is a very intriguing approach that will result in considerable cost savings and may have wide application outside of the linear collider area

At first glance the use of NMOS would appear to be a non-starter, since usually NMOS circuitry consumes more power than CMOS circuitry. However, in collaboration with Sarnoff we have developed a very compact logic that uses a switched capacitor array to form a resistive load for the logic. This arrangement has very low power consumption, compatible with the goal of 100 watts for the entire vertex detector.

The second prototype design was completed in the last quarter of 2011 and submitted for fabrication in a 90 nm process (see Figure 1). With the new NMOS design, the pixel size (with two memories) has been reduced to $25\,\mu\text{m} \times 25\,\mu\text{m}$ and is close to the final pixel size. In order to keep the power consumption of the comparator part of the in-pixel circuitry we have had to use some PMOS transistors. These transistors will compete with the charge collection node and cause some signal loss, but we still expect to collect at least 80% of the charge from the epilayer.

We received the first devices from the second production in June of 2012 and immediately began testing them. Following six months of testing and evaluating these devices, we began work with Sarnoff to design the third prototype.

The proper function of the novel NMOS in-pixel memory was demonstrated. It was also demonstrated that the new analog calibration scheme for each pixel was working as expected. The new design uses an analog circuit to store the comparator offset at the start of each bunch train; this currently has a precision of about 3 mV.

For the second prototype detectors we attempted to capitalize on the increased sensitivity we found with the first prototypes. By making the charge collection node smaller, we hoped to reduce the capacitance still further, with the limiting factor being the stray capacitance of the reset circuit. The desired increase in sensitivity in the second prototype was not achieved due to the layout of the charge collection node. The n-type charge node was implemented as a simple diode and the foundry's design rules required that it be surrounded by a highly doped p-type implant. We now believe that by implementing the charge node as a transistor, it is possible to evade the design rule for the highly doped surrounding p-type implant. This will reduce the capacitance of the charge collection node and promises to provide MIP sensitivity for the third-generation devices.

In order to stay within budget for the fabrication of prototype 3 we are again using the standard 7 μm low-resistivity epilayer that is available at TSMC through MOSIS. According to our simulations, the noise figure of the third prototype design with the thin, 7 μm epilayer will be sufficient to achieve 91% efficiency for minimum ionizing particles and a noise threshold 5 sigma above zero. For large-scale production of these devices a thicker epilayer with higher resistivity will be used, resulting in a better signal-to-noise ratio and therefore a much higher efficiency.

The development of prototype 3 by Sarnoff attempts to improve the device in the following ways:

1. Decrease sensor capacitance (Sarnoff calculations show a decrease by a factor of 10);
2. Reduce crosstalk: separate analog and digital power and ground, shield trace, connecting sensor to source follower input from busses, caring strobes and clocks (by changing metal layers designations);
3. Implement two-way calibration process;
4. Remove buffering of sensor reset pulse inside the chip. This will allow control of the amplitude of this pulse, which is especially important with decreased sensor capacitance;
5. Remove unnecessary multiplexing of time stamp (pure technical shortfall of prototype 2 design, which may limit speed and increase feedthrough noise);
6. Improve time stamp memory robustness (in prototype 2 about 1% of memory cells fail to record time stamps correctly).

For prototype 3, six different sensor options were implemented on the same chip; eight columns were allocated for each option:

1. Same as prototype 2, for comparison;

2. Deep NWELL diode in the window in p^{++} layer. This violates design rules, but a waiver for design rules was accepted by TSMC;

3. Shallow NWELL diode also in the window; this also violates design rules, but a waiver was accepted;

4. "Natural transistor" (NTN) allowed by design rules to be in the p^{++} layer window. The transistor is formed directly on p^{+} epilayer. Large source and drain diffusion areas, gate connected to both source and drain and form sensor output;

5. NTN also, but with two fingers, source and drain are narrow, gate also connected to both, as in option 4;

6. Same as 5, except gate is not connected to source and drain, but is connected to external bias voltage.

The tests for these six different configurations of the charge collection nodes will provide important generic information of a fundamental nature, useful in the future for other efforts, such as the LHC CMOS programs.

During the final months of this grant we received from Sarnoff Corporation [3] and began testing the third generation design (see Figure 2), which is again based on in-pixel NMOS circuitry and out-of-pixel CMOS elements for the interface logic.

Initial Prototype 3 Tests

Tests of prototype 3 were started during the grant period. After setting all power supply voltages and optimizing timing of the control signals, reliable time stamp recording in the pixel memories was

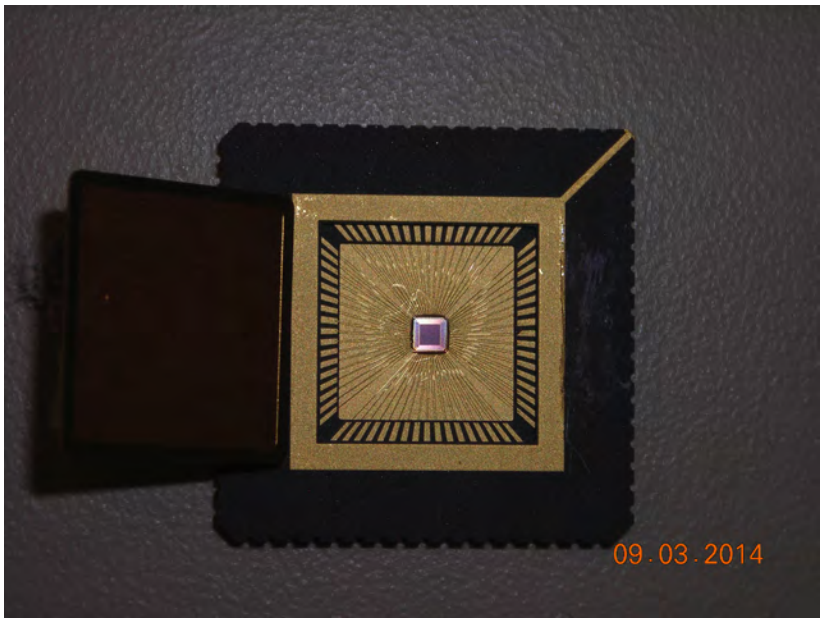

Figure 2: Image of third prototype. The chip size is 1.9 $\times$1.9 mm^2, working area is 1.2 $\times$ 1.2 mm^2 (48 $\times$ 48 pixels) and the pitch of the connection pads is 90 microns.

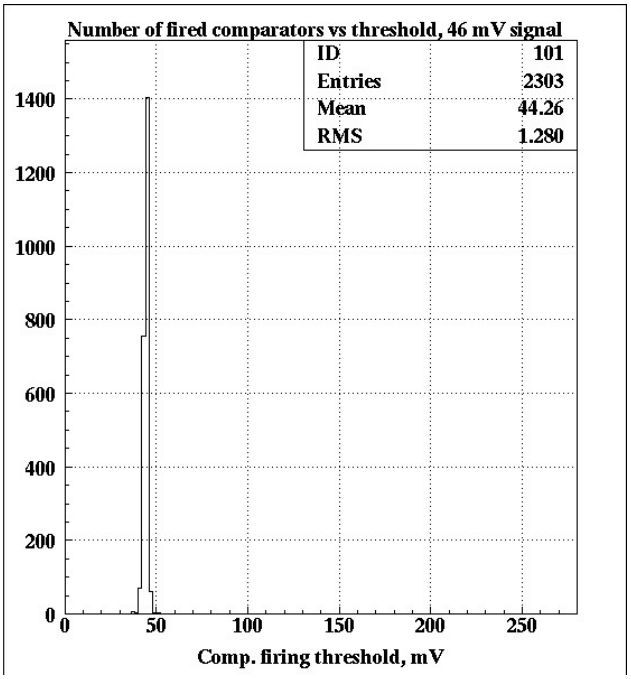

Figure 3: Distribution of prototype 3 comparator thresholds, showing an rms spread after calibration of 1.28 mV.

first achieved. The next test was to look at the performance of the comparator after application of compensation circuits. As can be seen from Figure 3 the distribution of the comparator thresholds after this compensation is very narrow, with an rms of 1.28 mV. This corresponds to the design expectation. A third test reveals a rough estimate of the sensor capacitance for each sensor option by observing the voltage change on the sensor due to coupling to the sensor reset pulse. The gate to source capacitance of the reset transistor is the same for all sensor options, and the voltage change depends only on the sensor capacitance - if it is smaller, the voltage change is larger. Figure 4 shows the value of this change for each pixel, with red indicating sensors with the largest values. The six types of sensors are clearly seen as the similar results in a vertical strip of sensors.

More accurate measurements of the sensor capacitance were obtained by observing ^{55}Fe signals (see Figure 5). The initial result shows a sensor capacitance that is reduced by a factor of 3 to 3.5 compared to prototype 2. This preliminary result comes from the the maximum signal seen in the sensor with a shallow NWELL diode, which violates (with waiver) the strict design rules. As shown in the figure, this sensor's (Option 3) signal reaches $\sim$100 mV; it was $\sim$ 28-30 mV in prototype 2 and $\sim$56 mV in prototype 1. Table 1 presents the sensor capacitances derived from the distributions shown in Figure 5.

Future tests will characterize the noise, charge collection efficiency, crosstalk and other features, including the time stamp information. Initial tests of time stamping are promising. These characterizations will be compared with detailed TCAD simulations.

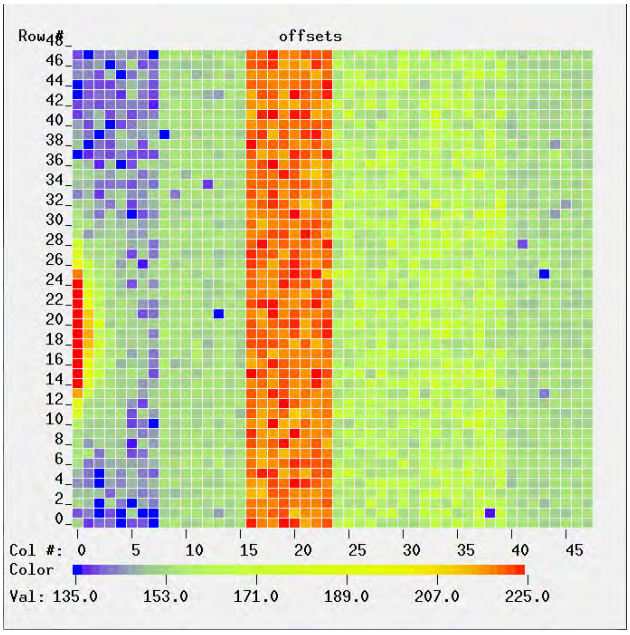

Figure 4: Voltage change due to reset, which is inversely proportional to the sensor capacitance (see text). The six different areas correspond to the six different charge collection nodes.

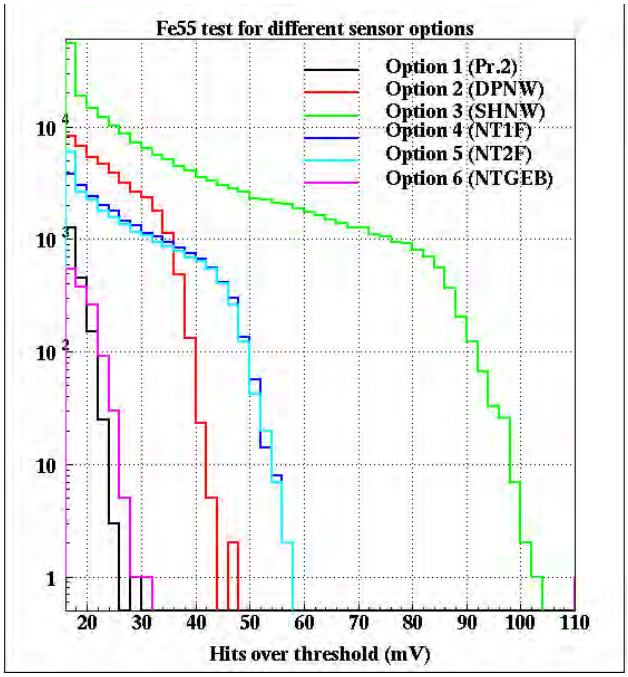

Figure 5: Distributions of ^{55}Fe signals from the six different sensor designs of prototype 3, defined in the text.

Table 1: Prototype 3 sensor capacitances for each option, determined from ^{55}Fe responses.

Option	Capacitance
1	9.0 fF
2	5.9 fF
3	2.7 fF
4 & 5	4.9 fF
6	8.9 fF

In summary, the remaining goals of this R&D program include the following:

- Finish characterization and testing of Sarnoff prototype 3 detectors using ^{55}Fe sources and lasers.
- Understand capacitance and noise associated with six different charge collection nodes and compare to detailed TCAD simulations of the charge collection nodes.
- Understand the charge collection efficiency of the detectors using radioactive sources and test beams.
- Explore TCAD simulations for detectors to be used in alternatives to the ILC machine such as the CLIC.
- Explore application of the Chronopixel technology to the LHC.

These tests represent a significant amount of work both on the test bench as well as in simulations. The broad plan of such tests and modeling are essential to develop a full understanding of the function of the various charge collection nodes.

1 Bibliography

References

[1] K. Abe, *et al.*, "Design and Performance of the SLD Vertex Detector, a 307 Mpixel Tracking System," Nucl. Instrum. Meth. A400, 287 (1997)

[2] N.B. Sinev *et al.*, "Second Chronopixel Detector Prototype," 2012 IEEE Nuclear Science Symposium, Anaheim, CA.;

C. Baltay, W. Emmet, D. Rabinowitz, J. Brau, N. Sinev and D. Strom, "Chronopixel Vertex Detectors for Future Linear Colliders," Proceedings of the DPF-2011 Conference, arXiv:1109.2811 [physics.ins-det];

N.B. Sinev *et al.*, "Test of the First Prototype of the Time Stamping Monolithic CMOS Pixel Detector," 2010 IEEE Nuclear Science Symposium, Knoxville, TN.

[3] Sarnoff Corporation, Princeton, NJ 08540-6449.

Research and Development for Precise Alignment of Future Lepton Collider Detectors

University of Michigan team:

- Keith Riles (Co-PI, Professor),
- Haijun Yang (Assistant Research Scientist)
- TianXiang Chen (Graduate Student)

The University of Michigan group carried out R&D toward the precise alignment of the inner tracking system and final-focus magnets for future high energy lepton collider detectors. Future lepton colliders will need extremely precise tracking of charged particles, to exploit fully the physics at TeV energies. A major systematic limitation will likely come from misalignment of tracking elements if conventional technologies used in previous electron-positron detectors are used. In addition, the *a priori* alignment of final-focus quadrupole magnets is critical at the International Linear Collider (ILC) with two detectors in a push-pull configuration, where the final sets of magnets travel with the detectors and must be rapidly restored to an absolute precision better than 50 μm, in order to allow beam-based alignment techniques to be used. Ideally, an alignment system should permit prompt "bootstrapping" of quadrupole and tracker positions following a detector move.

In this project, the Michigan group continued a program of alignment R&D based on Frequency Scanned Interferometry (FSI) in which a geodetic grid of points attached to the detector and to nearby bedrock is used to measure positions, rotations and distortions of detector and accelerator elements. In this scheme, the points in the grid are optically linked via a network of laser beams, using optical fibers for beam launching and collection. Small beam splitters and retroreflectors define interferometers for which a scanning of laser frequency over a known range defines absolute distance measurements to sub-micron precision. The basic FSI method was pioneered on the ATLAS detector by the group at Oxford [1, 2, 3].

The aim here was to build upon earlier Michigan 1-dimensional FSI measurements to establish true 3-dimensional reconstruction of position offsets at the required accuracy on an optical bench, using a multi-channel FSI system. The necessary additional components for the multi-channel system were purchased, assembled and tested. Measured performance met the specifications, confirming the general applicability of the FSI method. At the same time, the sizes of the components used, relative to earlier prototypes, were reduced, along a path toward ultimate miniaturization and lightening of material burden needed for the inner core of a linear collider tracking detector.

The Michigan group's research for this project built upon its prior exploratory single-channel, 1-dimensional studies, where sub-micron accuracy had been achieved under deliberately hostile environmental conditions. At the core of the FSI method are interferometers anchored to the objects for which alignment is the goal. The reference points for the interferometers are optically linked via a network of laser beams, using optical fibers for beam launching and collection. These points form a geodetic grid, where FSI

measurements determine absolute distances between pairs of points. The figure below shows a conceptual schematic diagram of a single FSI channel.

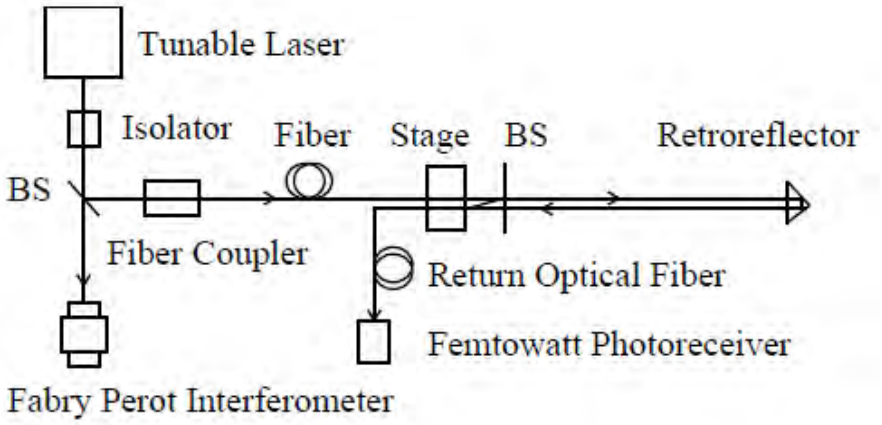

Schematic of a single-channel optical fiber FSI system

The Michigan group began R&D in this area in 2003 and published two articles [4, 5] describing progress in the 1-dimensional, single-channel configuration, for which the group achieved a precision of 200 nm on line-of-sight distances for ranges up to 40 cm, using optical beams of wavelength near 670 nm.

A primary goal of this project, which was met, was to demonstrate on a bench that 3-dimensional displacements of a object to which FSI reference points were attached could be reconstructed with sub-micron accuracy, using lighter-weight components than had been used in the 1-dimensional measurements. To establish this milestone, an 8-channel FSI system was assembled in the Michigan lab, where each channel consisted of an optical fiber mount with input and output fibers, a thin, low-reflectivity glass beam-splitter and a small metal retroreflector to create the interferometer. In practice, one of the channels did not work reliably, and measurements were based on up to 7 operational channels. The photos below show 3-channel and 5-channel configurations used for results reported at the October 2012 Linear Collider Workshop in Arlington, Texas [6]. For each channel, the absolute distance was defined to be the distance between the retroreflector and the fiber-launcher. More precisely, the distances between the retroreflector sides of the beam splitter and the inside vertex of the hollow corner cube used as the retroreflector were measured.

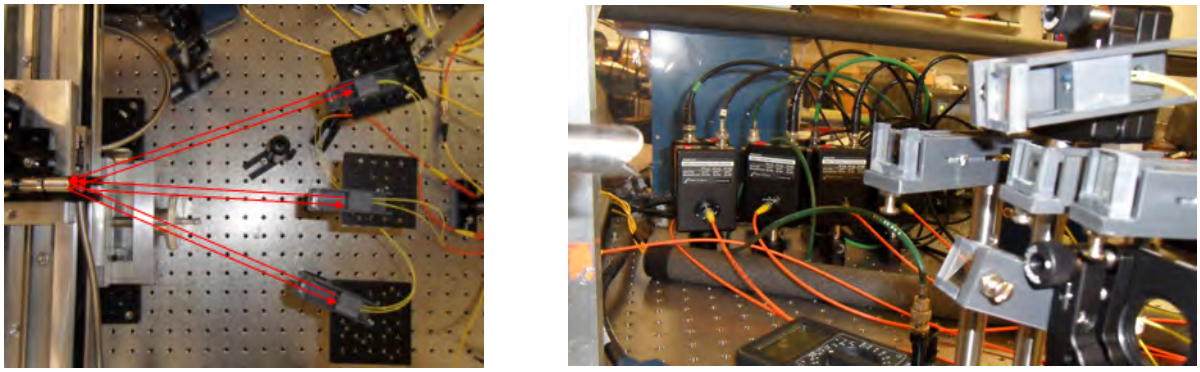

Photos of 3-channel and 5-channel configurations of the FSI test system
(arrows on left indicate paths of launched and returned laser beams)

In measurements, the "target" containing a small retroreflector was mounted on a 3-dimensional translational stage with 0.5-micron precision in the horizontal plane and 2-micron precision in the vertical direction. To measure ultimately achievable precision on 3-d position, the relative positions of the launchers to an arbitrary origin defined by the target's initial position were determined via eight displacements in the horizontal and vertical directions, and a least-squares minimization performed. With these launcher positions determined, new and larger displacements of the target were performed, and those displacements determined from the new FSI measurements and from the launcher positions determined previously. These measurements confirmed that for horizontal displacements, sub-micron accuracy was maintained up to 200-micron displacements from the origin, and for vertical displacements, measurements were consistent with the 2-micron uncertainty of the translation stage calibration [6]. These measurements confirmed the viability of the FSI method for precise absolute 3-dimensional positioning of detector and accelerator components.

Issues to address in future R&D include

1. Further miniaturization and material trimming of FSI components;
2. Improved beam light delivery and collection efficiency for extending FSI measurement lengths;
3. Extension to infrared laser wavelengths to exploit telecommunications technology;
4. Higher-bandwidth measurements for real-time alignment monitoring and correction; and
5. Efficient geodetic grid design.

References:

1. A.F. Fox-Murphy et.al, "Frequency scanned interferometry (FSI): the basis of a survey system for ATLAS using fast automated remote interferometry", Nucl. Inst. Meth. A383, 229-237(1996)
2. P.A. Coe et.al, "Frequency scanning interferometry in ATLAS: remote, multiple, simultaneous and precise distance measurements in a hostile environment", Meas. Sci. Technol.15 (11): 2175-2187 (2004)
3. S.M. Gibson et.al, "Coordinate measurement in 2-D and 3-D geometries using frequency scanning interferometry", Optics and Lasers in Engineering Volume 43, Issue 7: 815-831 (2005)
4. Hai-Jun Yang et.al, "High-precision Absolute Distance and Vibration Measurement using Frequency Scanned Interferometry", Applied Optics, Vol.44, 3937-3944(2005). [Physics/0409110]
5. Hai-Jun Yang et.al, "High-precision Absolute Distance Measurement using Dual-Laser Frequency Scanned Interferometry under Realistic Conditions", Nucl. Instrum. & Meth. A575 (2007) 395-401. [Physics/0609187]
6. Keith Riles, Hai-Jun Yan and Tianxiang Chen, "Update on FSI R&D for Final Focus Magnet and SiD Tracker Alignment", presentation at Linear Collider Workshop 2012, University of Texas, Arlington, October 2012.

Linear Collider R&D Report UCSC/SCIPP

During the course of the funding period, the group at the Santa Cruz Institute for Particle Physics (SCIPP) worked both on enabling instrumentation R&D geared towards the development of Linear Collider detectors, as well as simulations geared towards the design and optimization of the detectors.

1. Instrumentation Studies

The thrust of the instrumentation activity was focused on proof-of-principle studies of various prospective approaches to particle detection and measurement at the ILC.

1.1 Use of charge division for determining the longitudinal coordinate for strip electrodes

A prior SCIPP tracking simulation study [1] showed a significant reduction in the number of fake particle tracks that originate within the detector volume if a longitudinal resolution of ~1cm or better is achieved. Based on a suggestion by V. Radeka [2], we explored the longitudinal resolution properties of a discrete resistive network similar to that of a resistive silicon-strip detector electrode (such as that provided by an un-metalized implant) read out on both ends by independent charge-sensitive amplifiers (see Fig. 1).

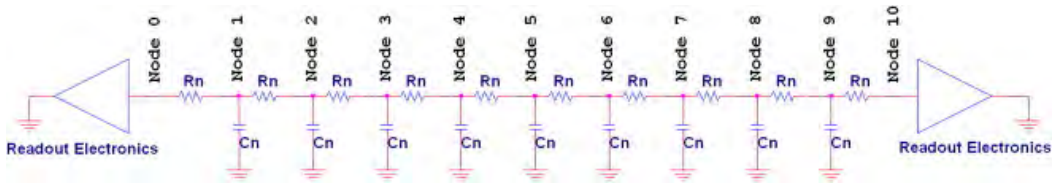

Fig. 1: Discrete component network used to approximate a resistive silicon diode detector electrode read out on both ends by independent charge-sensitive amplifiers.

Shown in Fig. 2 is the charge division achieved after optimization of the readout. For a 10cm-long electrode, the fractional resolution of 0.06 corresponds to a 6mm longitudinal position resolution, better than the 1cm figure-of-merit cited by [1]. This work was published in Nucl. Instr. & Meth. (see publication [PR1]) and is being explored as a possible readout option for the ILD silicon strip system.

1.2 Length limitations for microstrip electrodes use to read out minimum-ionizing particle detectors

In the case of the ILC, for which the beam-delivery and detector-occupancy characteristics permit a long shaping-time readout of microstrip sensors, it is possible to envision long (~1 meter) daisy-chained 'ladders' of fine-pitch sensors read out by a single front-end amplifier. A study was conducted at SCIPP for which a long shaping-time (~2μsec) front-end amplifier was used to measure readout noise as a function of detector load. A comparison of the measured noise to that expected from lumped and distributed models of the load network showed that network effects significantly mitigate the amount of readout noise contributed by the detector load. Figure 3 shows the comparison between measured noise and that expected for both the naïve lumped-element approximation as well as that derived from a full network simulation, the latter of which closely reproduces the measured noise levels.s

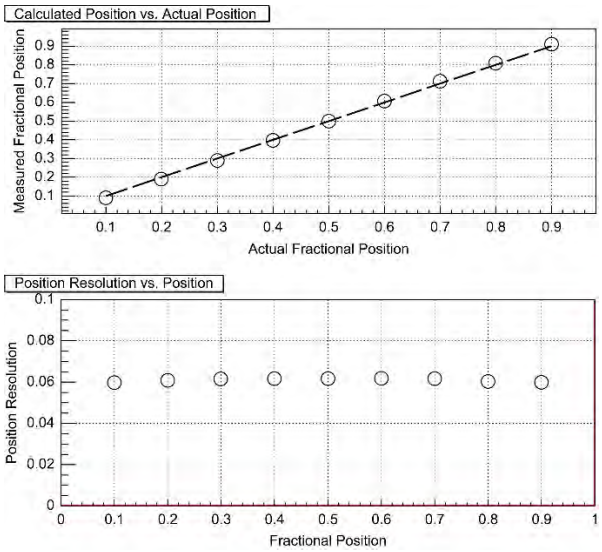

Fig 2: Charge-division response as a function of electrode node (upper) and fractional position resolution (lower) observed for the discrete network approximation of Fig. 1.

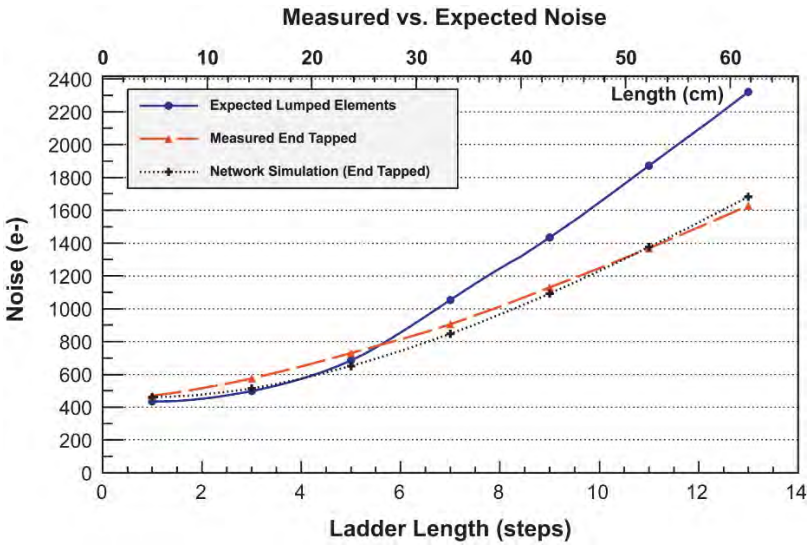

Fig. 3: Measured noise as a function of ladder length for narrow-strip sensors appropriate for achieving ILC-level position result; each step is 4.75cm in length, with an electrode width of 7µm. Also shown is the expectation under the assumptions of lumped elements (blue) and from a full network simulation of the electrode transmission line (dotted). A significant reduction in electronic noise is seen to be attributable to network effect.

Combining the measured results with a pulse-development simulation developed at SCIPP, a maximum ladder length of 75 cm was estimated for a ladder composed of these sensors that is intended to detect minimum-ionizing particles. Further reduction in noise was observed for the case that the sensor load is read out from its center rather than its end, with a corresponding increase in maximum ladder length to approximately 95 cm. This work was also published in Nucl. Instr. & Meth. (see [PR2]).

1.3 Electromagentic radiation damage to solid state sensors

Detectors proposed for the International Linear Collider (ILC) incorporate a tungsten sampling calorimeter (`BeamCal') intended to reconstruct showers of electrons, positrons and photons that emerge from the interaction point of the collider with angles between 5 and 50 milliradians. For the innermost radius of this calorimeter, radiation doses at shower-max are expected to reach 100 MRad per year, primarily due to minimum-ionizing electrons and positrons that arise in the induced electromagnetic showers of e+e- `beamstrahlung' pairs produced in the ILC beam-beam interaction. However, radiation damage to calorimeter sensors may be dominated by hadrons induced by nuclear interactions of shower photons, which are much more likely to contribute to the non-ionizing energy loss that has been observed to damage sensors exposed to hadronic radiation.

To this end, we proposed and ran SLAC Experiment T-506, for which several different types of silicon diode sensors were exposed to calibrated doses of radiation induced by showering electrons of energy 3.5-10.6 GeV. By embedding the sensor under irradiation within a tungsten radiator, the exposure incorporated hadronic species that would potentially contribute to the degradation of a sensor mounted in a precision sampling calorimeter. Four types of silicon sensors were explored: both Magnetic Czochralski and Float-Zone for n-type and p-type bulk, with exposures of up to 220 MRad. Figure 4 shows the charge-collection efficiency for n-bulk Czochralski sensors as a function of reverse bias voltage before irradiation and after doses of 90 and 200 MRad. Good charge-collection efficiency was maintained at even the highest dose. These results were also published in Nucl. Instr. & Meth (see [PR1]). Subsequently, a GaAs pad sensor was also given a 6 MRad exposure; even at this low level, it exhibited a charge collection degradation of approximately 20%.

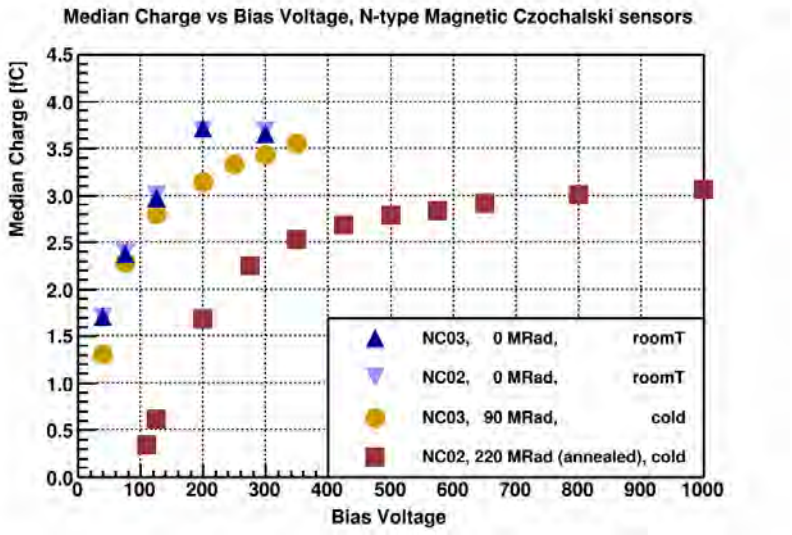

Fig. 4: Charge-collection efficiency results for n-bulk Magnetic Czochralski sensors at high dose.

2. Simulation Studies

Two significant simulation studies were performed during the funded period: one having to do with exploring the tracking capability of tracker with only ten layers and the other with the performance of the BeamCal amidst high electron-positron pair backgrounds from the beam-beam collision.

2.1 Non-prompt track reconstruction

With its small number of precise tracking layers, the question of reconstruction non-prompt tracks has been an ongoing concern for the SiD Detector. The SCIPP group performed a study of tracks arising from the non-prompt decay of staus to tau plus gravitino. Figure 5 shows the reconstruction efficiency for tracks arising from the subsequent decay of the tau lepton as a function of decay radius, for tracks arising at radii lying within the second layer of the inner tracker. Good efficiency is maintained even to high radii of origination. The results of this study have been published in the proceedings of LCWS11, Granada, Spain, September 2011.

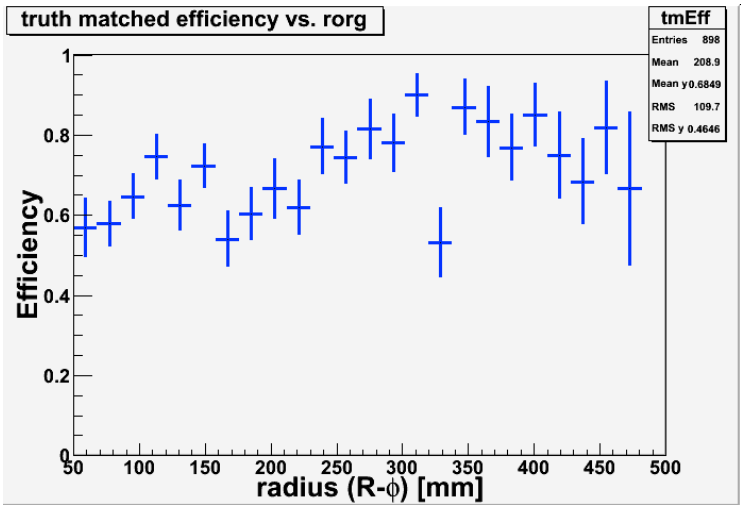

Fig. 5: Reconstruction efficiency for tracks arising from non-prompt stau decay, as a function of radius of origination of the track.

2.2 BeamCal segmentation strategy

Beam-beam backgrounds due to incoherent electron-position pair production increase rapidly with decreasing radius from the beamline, leading to the possibility that a radially-varying segmentation of the BeamCal may provide better performance than a fixed segmentation size over the full radial extent of the BeamCal. After developing and validating a reconstruction algorithm for the simulated BeamCal instrument, the SCIPP group explored to variants of the segmentation scheme: one with fixed segment size and one for which the segment size became finer as radius decreased. Figure 6 shows the overall BeamCal reconstruction efficiency for 50 GeV electrons for various overall segmentation scales for the fixed and radially-varying segmentation, as a function of the total number of channels. The radially-varying scheme is found to be somewhat more efficiency per channel for the reconstruction of these relatively low-energy electrons.

Peer Reviewed Publications

[PR1] Initial Results of a silicon sensor irradiation study for ILC extreme forward calorimetry, R. Band et al., Nucl. Instr. & Meth., DOI: 10.1016/j.nima.2014.04.041, 2014.

[PR2] Microstrip electrode readout noise for load-dominated long shaping-time systems, K. Collier et al., Nucl. Instr. & Meth. A729:127, 2013.

[PR3] Longitudinal resistive charge division in multi-channel silicon strip sensors, J. K. Carman et al., Nucl. Instr. & Meth. A646:118, 2011.

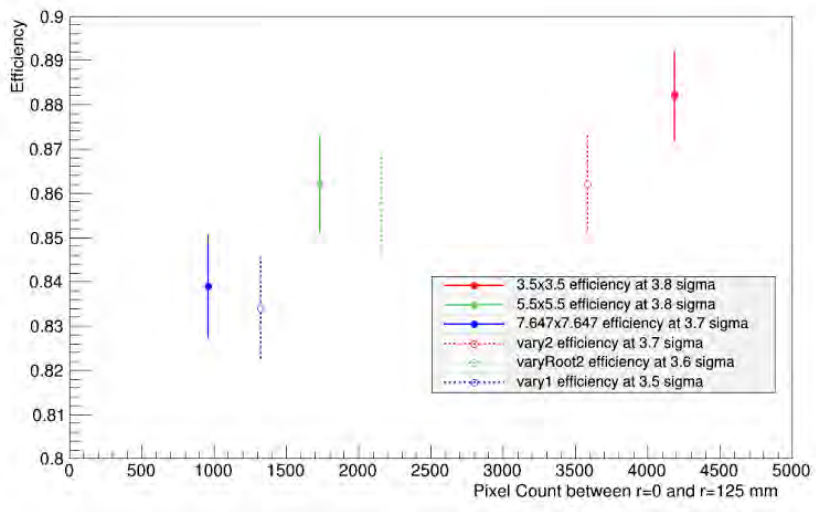

Fig 6: Overall reconstruction efficiency for 50 GeV electrons as function of channel count for fixed (solid) and radially-varying (dotted) BeamCal segmention.

Conference Proceedings

[CP1] Initial result of a silicon sensor irradiation study for ILC extreme forward calorimeter, R. Band et al., International Workshop on Future Linear Colliders, 11-15 Nov. 2013, Tokyo, Japan; eprint arXiv:1402.2692 [physics.ins-det

[CP2] Generic microstrip R&D topics at SCIPP: longitudinal charge division and length limitations for long ladders, J. Carman et al., Proceedings of the International Workshop on Future Linear Colliders (LCWS11), Granada, Spain, 26-30 September, 2011; eprint arXiv:1112.4823 [physics.ins-det].

[CP3] Metastable staus: reconstructing non-prompt tracks at the ILC with the SiD detector, C. Betancourt, F. Bogert and B. Schumm, Proceedings of the International Workshop on Future Linear Colliders (LCWS11), Granada, Spain, 26-30 September, 2011; eprint arXiv:1112.4825 [physics.ins-det].

[CP4] Developments in Readout for Silicon Microstrip Sensors at a Linear Collider Detector. Jerome Carman et al., Proceedings of International Linear Collider Workshop 2010 (LCWS10 & ILC10), Beijing, China, 26-30 Mar 2010; e-Print: arXiv:1005.2623 [physics.ins-det]

Invited Talks

Spanish Network Workshop on Future Linear Collider, University of Sevilla, February (via WEB)

- *Silicon Microstrip R&D at SCIPP and the University of California at Santa Cruz*

LCWS13 (2013 International Workshop on Linear Colliders) Tokyo, Japan, November

- *Limitations on Microstrip Ladder Length*
- *Initial Results from the SLAC ESTB T-506 Irradiation Study (delivered in two separate sessions)*

FCAL Collaboration Meeting, Zeuthen, Germany, October (via WEB conferencing)

- *Initial Results from the SLAC ESTB T-506 Irradiation Study*

LCWS11 (2011 International Workshop on Linear Colliders) Granada, Spain, September

- *Reconstructing Non-Prompt Tracks with the SiD Detector*
- *R&D on Tracking at UCSC / SCIPP*

2011 Linear Collider Workshop of the Americas, Eugene, OR, March

- *Update on Linear Collider Tracking R&D at SCIPP*

2010 European Community Workshop on Linear Colliders, Geneva, Switzerland, October

- *Use of Silicon Diode Sensors for the Beamline Calorimeter*
- *Tracking R&D at SCIPP*
- Physics Seminar, San Jose State University
- *Linear Collider Research and Development at SCIPP*

2010 International Linear Collider Workshop, Beijing (remote attendance), March

- *Fundamental Microstrip R&D at SCIPP*

References

[1] C. Meyer, T. Rice, L. Stevens, and B. A. Schumm, *Simulation of an all-silicon tracker*, ECONF C0705302:SIM09, arXiv:0709.0758, September, 2007.

[2] V. Radeka, IEEE Transactions on Nuclear Science **21** (1974), 51.

April 21, 2015

Powering of ILC Detector Front End Chips by DC-DC Converters & HV RF

Satish Dhawan, Yale University

The front end readout chips for the ILC (KEPiX) are fabricated with 250 nm technology requiring operating voltages of 2.5 V. The next generation of readout chips will be in 180 nm technology, requiring voltages of approximately 1.2 V. We have explored the delivery of 48 Volts to inside the detector near the front end where it is converted to 12 V by DC-DC converters, followed by a second stage close to the KEPiX chips where the 12 V is converted to 1.2 V.

We are using a Buck converter circuit topology in which a single power chip with only one external air core inductor is used along with a few passive components. In this circuit, the inductor is charged to store energy that can be withdrawn over a longer period of time. This is effectively a DC transformer. The output power is at a lower voltage but higher current. The conversion efficiency depends upon the input/output voltage ratio and the operating frequency. Any power loss in the converter adds to the cooling load, so the highest possible efficiency is required.

The physical size of the inductor and the capacitors decrease with frequency. It is advantageous to go to higher frequency to reduce the space needed by the converters. There are very few (if any at all) non-physics applications that require DC-DC converters in high magnetic fields. Commercial applications use magnetic material in the inductor and are limited to less than 1 to 2 MHz.

High band gap (GaN) devices can operate at much higher frequencies and with higher efficiency than those made with silicon. Our tests on GaN FETs have shown that the transistors are very radiation hard – much harder than the requirements of the ILC experiments.

Since the ILC duty cycle is very low, turning on power only when needed is desirable to lower power loss. We have tested this and found that when the power is switched off quickly, it can produce an overshoot on the output that can exceed the voltage rating of the KEPiX chips. For example, 1 Ampere flowing thru the last segment of the power delivery cable with 10 ohm impedance will produce 10 Volts overshoot when the power is shut off. Lower characteristics impedance and slower turnoff are the obvious things to look at to control the overshoot.

Drawings & Photos at the Web Page
Yale webpage: http://shaktipower.sites.yale.edu/seminars

Publications:

Detector Powering in the 21st Century - Why stay stuck with the Good old 20th Century methods?, S. Dhawan and R. Sumner, TIPP (Technology and Instrumentation in 2011 Conference 9-14 June, 2011 Chicago, Il. Physics Procedia 37 (2012) pages 181–189

Powering of ILC Detector Front End Chips by DC-DC Converters. S.Dhawan, O.Baker, H.Smith, P.Tipton, H.Chen, J. Kierstead, F. Lanni, D.Lynn, S.Rescia, M.Weber, C.Musso, A. Mincer, R. Khanna" Proceedings of IEEE NPSS Real Time Computing Conference Beijing, China / May 10 - 15, 2009

Progress on DC-DC Converters for Si Tracker for the sLHC Upgrade. S. Dhawan, O. Baker, R. Khanna, J. Kierstead, D. Lynn, A. Mincer , C. Musso, S. Rescia, H. Smith, P. Tipton and M. Weber, Proceedings of the 2009 Topical Workshop on Electronics for Particle Physics, Paris, France

Talks:

12-14 January 2015: **Progress on Powering Options**; SiD workshop, SLAC

12-16 May 2014: **Powering of Detector Systems**; AWLC 2014, Fermilab,

17-19 April 2013**: Powering Future Particle Physics Detectors**,
Joint CPAD Snowmass Instrumentation Frontier meeting, Boulder, Colorado.

9-11 January 2013: **Power Delivery for Future Experiments**, Instrumentation Frontier Community Meeting (CPAD), Argonne National Laboratory, Argonne, IL.

16-18 November 2012**: Why DC-DC Converters for High Energy Physics,** PowerSoC2012: The 3rd International Workshop on Power Supply on Chip, San Francisco, CA

03 October 2012: **Why Physics experiments need GaN based DC-DC Converters**?
AIST: Advanced Industrial Science & Technology Center, Tsukuba, Japan

01 October, 2012: **Report on DC-DC Converters for HEP and the Role of GaN FETs**
KEK Detector Technology Seminar, Tsukuba, Japan.

19 – 23 March, 2011: **Testing of Cables for KPiX Pulse Load**, ALCPG, , University of Oregon, Eugene, OR.

15-17 November 2010: **Powering Delivery to KPiX Chips**, SiD Workshop, University of Oregon, Eugene, OR.

Final report, UNM contribution, DOE SiD R&D grant

Sally Seidel and Martin Hoeferkamp
9 April 2015

The University of New Mexico group proposed to design, prototype, and test low mass readout cables to connect tracker modules to the concentrator boards at the end of the SiD barrel. The specifications required minimum achievable radiation length, total resistance less than 1 ohm for each power plus ground pair, and cable width below 1 cm. The cable was initially designed with two elements: a short pigtail that attaches directly to the module, and a longer extension cable that connects the pigtail to the concentrator. The pigtail required the most R&D, as it includes bias tabs and surface-mount pads for bias and power filtering in addition to traces for analog and digital power, digital control and readout, and sensor bias. The extension cables are conceptually simpler but must be manufacturable in production quantities with lengths up to 2 meters. A small adaptor board was also designed to permit testing of the pigtail on a test stand prior to completion of the extension cable.

The cable system described above was realized in two layers, prototyped, and tested. TDR measurements at UNM demonstrated that the 100 ohm differential pair impedance requirement was met. Connectivity tests confirmed that the product can be produced with very high yield. Parts were soldered onto the cable at UNM with no problems. Cirexx and Vector Fabrication produced the pigtails. Q-Flex produced the extension cable.

Several problems external to the cable itself required design revisions after proof-of-principle had been achieved. Problems with the sensor surface led to abandonment of the plan to wirebond the pigtail to the sensor. At the time of this writing, the full complement of tested and working cables has been transferred from UNM to the team at SLAC working on integration. That team is examining several connection methods including solder bumps. A technical limitation on the UC Davis flip-chip facility required that the original pigtail be split into two parallel "semi-pigtails," each carrying half the connections to the extension cable. This longitudinal split improves the isolation of the chip, suppressing noise and crosstalk, although this was not a motivating factor in the modification. The semi-pigtails have lengths 78 and 92 mm, combined width 8mm, and thickness 250 microns. The extension cable was produced at length 0.5m.

Project Final Report

April 2015

Development of a Silicon-tungsten Test Module for an Electromagnetic Calorimeter

Personnel and Institutions which were funded

University of Oregon, Department of Physics and Oregon Center for HEP:
Jim Brau, Raymond Frey, David Strom, Craig Gallagher,
graduate students: William McCann, Dylan Mead, Peter Radloff,
undergraduate student: Kyle Travis

University of California, Davis, Department of Physics:
Richard Lander, Mani Tripathi, Britt Holbrook, Christian Neher,
graduate student: Michael Woods

Other Collaborators

Stanford Linear Accelerator Center:
M. Breidenbach, D. Freytag, N. Graf, G. Haller, R. Herbst, J. Jaros, T. Nelson

Brookhaven National Lab:
V. Radeka

Project Contact

Raymond Frey
rayfrey@uoregon.edu
541-346-5873

1 Overview

Innovations in integrated readout electronics, interconnect technologies, and silicon sensors have provided an opportunity for developing dense, highly-segmented electromagnetic sampling calorimeters (ECal) using alternating layers of silicon readout and tungsten radiator. This project has used our expertise in interconnects and silicon detectors in high-energy physics to develop an ECal prototype. The silicon sensors, combined with very compact interconnects and readout, allow a very small readout gap (≈ 1 mm) between tungsten layers, thus giving a small Moliere radius. A prototype module employing this technology was placed in a beam line at SLAC in 2013 and fully exercised.

This represents a proof of principle which enables confident development of compact, imaging electromagnetic calorimeters, in which showers are confined to a small volume, photons can be easily identified with respect to charged particles, and non-showering charged particles can be tracked. A key element of this project has been that — in transverse and longitudinal segmentation, and in its integrated approach to readout — the prototype closely mimics designs which might be employed in a real collider detector.

This technology would enable the successful implementation of imaging electromagnetic calorimeters in future collider detectors which rely on excellent pattern recognition with good energy measurement in a compact package. Thus, superb measurement of jet or tau final states using particle-flow or similar algorithms would be well matched to this ECal. Our design was optimized for the ECal of the SiD detector concept of the ILC, and Table 1 gives some design parameters for the ECal as envisioned for SiD. However, the basic technology is widely applicable. In fact, the CMS collaboration at the LHC has recently decided to use a silicon-tungsten technology for its endcap upgrade.

Table 1: Global silicon-tungsten ECal parameters.

longitudinal profile	(20 layers $\times$ $0.64X_0$) + (10 layers $\times$ $1.3X_0$)
EM energy resolution	$0.17/\sqrt{E}$
silicon sensor segmentation	1024 hexagonal pixels
pixel size	13 mm^2
readout gap	1 mm (includes 0.32 mm thick Si sensors)
effective Moliere radius	13 mm
pixels per readout chip	1024
pixel dynamic range requirement	$\sim$ 0.1 to 2500 MIPs
heat load requirement	20 mW per sensor

This report is organized as follows: The next section describes the research and development of the interconnect technologies needed for this prototype, and the subsequent section briefly discusses the test beam and results. Finally, we discuss lessons learned and potential next steps.

2 Interconnect Development at UC Davis

There were two important components to finding interconnect solutions. The first was the bump bonding of the KPiX chip to the silicon sensors. The second was the flex cable which brings power and control signals from the edge of a module to the KPiX chips in a layer and transmits the single digital output from KPiX to the module edge. A somewhat detailed discussion of this follows.

2.1 Bump Bonding Development

During 2009-10, we had successfully demonstrated gold-stud thermo-compression bonding on dummy chips and resistances of about 10 mΩ per bump were obtained. However, when the technique was applied to the KPiX-Sensor wafer combination, it was discovered that the field-oxide on the sensor wafer could not withstand the pressure (up to 200g per bump) required for successful thermo-compression. Hence, gold-stud bonding was set aside until the vendor of sensor wafers could improve oxide strength.

The focus in 2010-11 was shifted to solder-ball bonding. We worked with a vendor, CVI, who had expertise in placing solder balls on chips. A polyimide film is applied to the chip and windows are opened to expose the bond pads. If the pad surface is aluminum (as is the case for KPiX), a "zincate" treatment of the bond pads removes the native oxide layer and facilitates it for Au-Ni plating. Special masks were made for this process for placing solder balls on our custom "dummy chips", which we use for evaluating bump-bonding technologies. These chips allow for an array of 20 bump-bonds that can be probed using another set of 40 bump-bonds and traces that run to the periphery. This set-up allows for 4-point measurements of the bump resistance. Figure 1 (top) is a picture of such an array with solder balls placed on the pads.

We obtained equipment for flip-chip alignment and solder re-flow, via another DOE grant at UC Davis and developed the technique by tuning bonding parameters. Figure 1 (bottom) is a photograph of the edge-view of a dummy chip combination once it is aligned. The next step consists of gently lowering the chip and heating the bottom chip, while the top chip is held apart at an optimal distance allowing the solder balls to melt and then cool, thus completing the bonding process.

We used two different solder types in the assembly. The first one had a higher temperature solder (eutectic Pb-Sn) which was used to attach the KPiX chips to the Hamamatsu sensor wafers. This solder had a liquidus temperature of 183C. Following that attachment, we used a lower temperature solder (eutectic In-Ag), with a liquidus temperature of 143C,for attaching the flex cable to the sensor wafer. Both of these solder types were evaluated and the results are shown in Figure 2. As is evident, both solders yielded an average bump resistance well below 10 m , which was easily acceptable for our purposes. The KPiX-A chips (1024 channels) were produced with eutectic Pb-Sn solder balls placed by the vendor, TSMC.

2.2 Flex Cable Development and Bonding

We went through several iterations of the flex cable design, for use with the version 2 sensor wafers from Hamamatsu. The necessary changes consisted of a new configuration for the cable attachment pads, a new outline of the wafer that was somewhat smaller with clipped corners, bond pads at the corner for guard rings and wafer bias, and a change in the connector type at the far end of the cable. Several other improvements were made such as a re-distribution of the power and ground planes to provide a shield next to the wafer, composed of the AVDD power plane. These cables were fabricated in 2011. The thickness of the cables was reduced by using a 2 mil dielectric instead of a 5 mil dielectric.

We have carried out bonding of flex cables to dummy hex wafers successfully, using the solder ball technique. Since the alignment requirements are less stringent in this case, a jig for this process was made in the physics department machine shop at Davis. While this jig proved to be adequate, we also

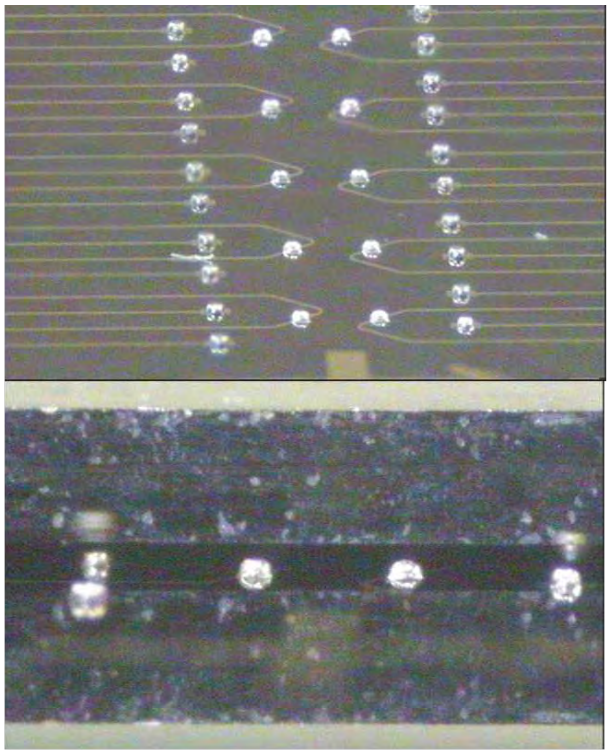

Figure 1: Array of solder ball bumps on one of the dummy evaluation chips (top) and a side view of the bumps after the top and bottom chips are aligned on the bonder (bottom). The solder is re-flowed with the top chip free-floating.

experimented with using the flip-chip aligner-bonder for this attachment, with good results. Figure 3 (top) shows the layout of the dummy hex wafers and the scheme for making two-point measurements of the cable to wafer bonds.

Figure 3 (bottom) shows the flex cable aligned to the dummy hex wafer just before re-flow. However, unlike the case of dummy chips, accurately maintaining the gap during re-flow was not possible in this case because the two tongues of the cable needed to be pressed down in order to make proper contact with the wafer. A special shim, attached to the top tool of the flip-chip aligner-bonder, was used for this purpose. Adequate results have been obtained, but further trials are ongoing to establish good repeatability of this procedure. Firgure 4 shows an edge view of the cable to wafer attachment just prior to the re-flow. Since this set-up only allows for 2-point resistance measurements, it was difficult to assess the bonds directly. However, we obtained values of 5-8 ohms which are consistent with trace resistances.

2.3 Fabrication of a prototype Si-W Calorimeter

The first step in this assembly consisted of attaching KPiX chips to hexagonal sensor wafers. Figure 5 (top) shows an example of the solder re-reflow process. A KPiX chip is shown being attached to a Hamamatsu sensor wafer. Bumps can be seen to reflow and form connections, with a reduction in their height. This process relies on having a pad surface with nickel and gold layers in order to form good low resistance connections. The sensor wafers from Hamamatsu had aluminum as their pad metal and presented a problem because of the presence of an aluminum oxide layer. We worked with a vendor (IZM, Berlin) to treat this surface using an electro-plating process. Figure 5 (bottom) shows a KPiX chip attached to the sensor

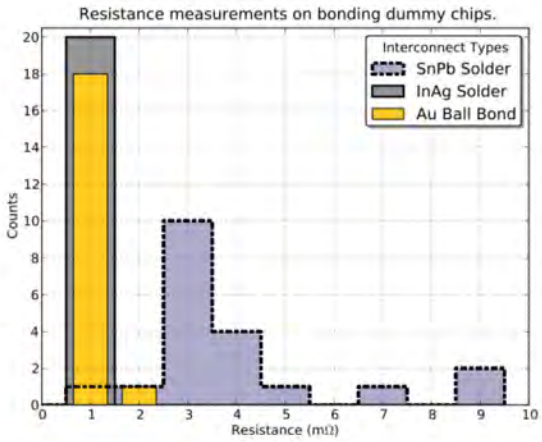

Figure 2: A histogram of 4-point measured resistance per bump obtained with gold studs and two types of eutrctic solders. All 20 of these bumps, for each technology, are acceptable.

wafer. This work was done by Neher and Woods working with Holbrook.

Figure 6 (left) shows an assembly with the KPiX and the hex Hamamatsu wafer. These assemblies were tested with a loop-back 4-point resistance measurement on a set of pads that allowed for this procedure. The probe station photograph for this is shown in Figure 6 (right). All bonds showed negligible resistance, much smaller than the inherent trace resistance of about 1 ohm. These were acceptable to the collaboration and the chips functioned properly.

The second step consisted of attaching the flex cables, which had low-temperature indium solder deposited on their pads, as shown in Figure 7. The solder bumps were well-defined and had a diameter of about 200 μm. The flex cables were attached to the assembly using our bump bonder. However, the remaining task of attaching the corner pads (which provide bias and grounds for the guard rings) called for the use of anisotropic conducting film (ACF). We also had to build a special jig for this purpose. Figure 8 (left) shows the procedure for local heating of the ACF at the corners. Due to differences in the coefficients of thermal expansion between silicon and kapton, care had to be taken to prevent bonds from coming apart after cool-down. As shown in Figure **??** (right), the cable has slots cut into it to prevent such an outcome.

3 Prototype and Test Beam

The primary goal of the R&D was to develop a module employing the technologies *as they would be implemented in a real detector*, as discussed above. A schematic of the module is shown in Fig. 9.

The program called for fabricating 30 such assemblies to instrument a calorimeter prototype. However, we did not have enough sensor wafers and we completed a total of 15 assemblies, out of which 13 were usable. Another 4 developed problems due to a manufacturing mistake. The remaining 9 good sensor layers were assembled into the calorimeter prototype at SLAC. There were 8 interspersed layers of tungsten as absorber — the entire stack summed up to about 6 radiation lengths.

The new End Station A test beam facility was seen as an ideal venue for the beam test. SLAC has the advantage that the beam naturally carries the timing structure of a linear accelerator, which underlies

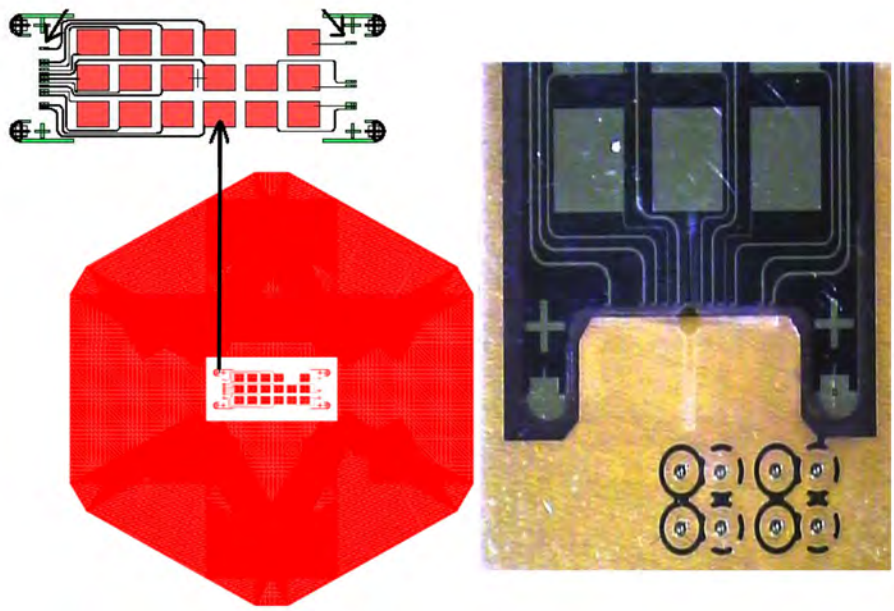

Figure 3: (Left) layout of the dummy sensor wafers with the cable attachment pads. The inset shows the details of the traces leading to probe pads in the center. These are used for 2-point resistance measurements. (Right) A photograph showing one of the two tongues of the flex cable after alignment to the dummy wafer below.

the timing characteristics of the KPiX chip. In addition, the SLAC beam has excellent collimation and stability characteristics. Finally, it is straight forward for the beam to deliver an average of 0, 1, 2, 3, ... electrons (or positrons) per pulse.

The prototype calorimeter was installed in End Station A, and saw a 4-day running period July 26-29, 2013. The 12.1 GeV beam was well-defined and contained 0.5 to 5 electrons per pulse. We met the basic specifications in terms of linearity, noise, gains etc for the electronics. Figure 10 is a typical image of an electron showering in the prototype with the event display developed by the Oregon students. While 6 radiation lengths does not allow sufficient containment to obtain good energy measurement, our measurements of the shower development are consistent with expectations, as can be seen in Figure11.

A unique and interesting measurement possible with our short stack is the two-shower separation. This capability is crucially important for imaging calorimetry at colliders, where separating the individual particles' contributions to jet energy, for example, is the basis for optimized techniques such as "particle

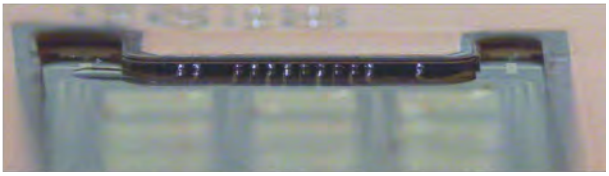

Figure 4: A histogram of 4-point measured resistance per bump obtained with gold studs and two types of eutrctic solders. All 20 of these bumps, for each technology, are acceptable.

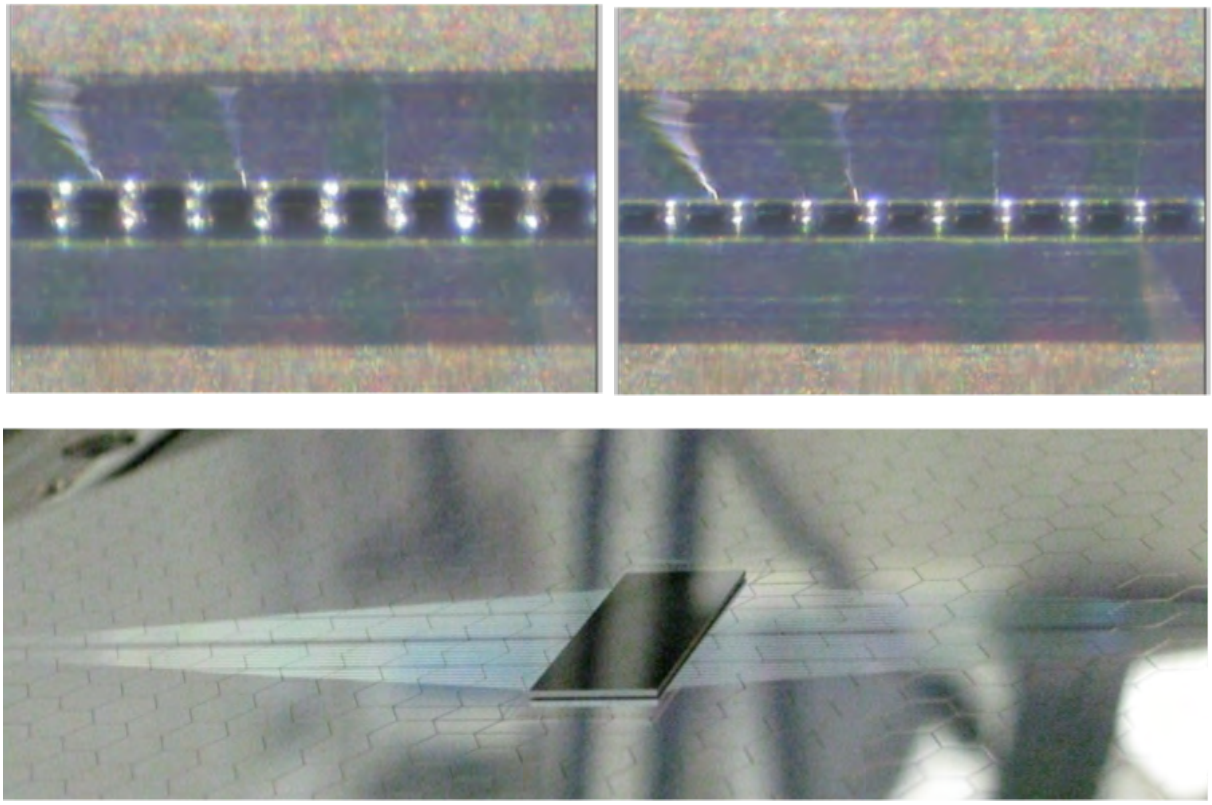

Figure 5: (Top) The reflow process in solder bump-bonding. Individual solder balls and their reflection can be seen on the left (before heating). On the right (after heating) they attach to pads and form bonds. (Bottom) A KPiX chip attached to a sensor wafer after re-flow.

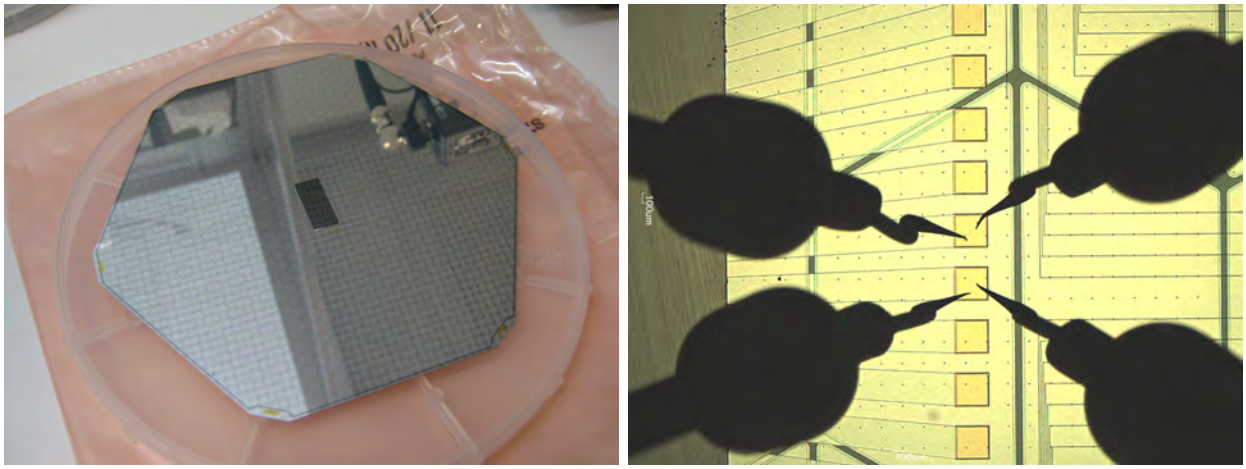

Figure 6: Left: A photograph of the Hamamatsu hex wafer with a KPiX chip bump-bonded to it. Right: A Photograph of the 4-point loop-back resistance measurement scheme.

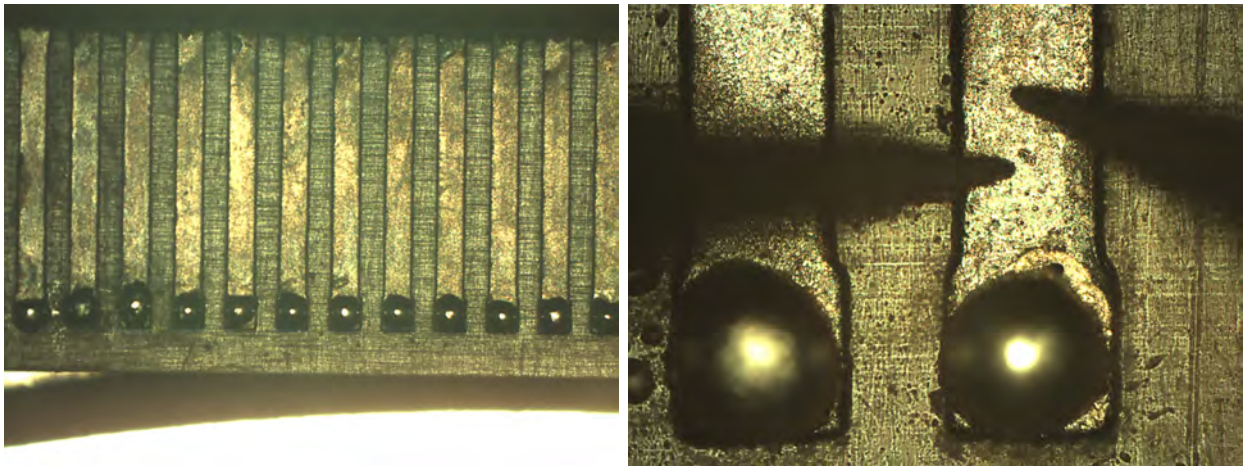

Figure 7: Left: Photographs of solder balls placed on the cable pads and re-flowed. As shown on the right, the balls are well defined and have a diameter of about 200 μm.

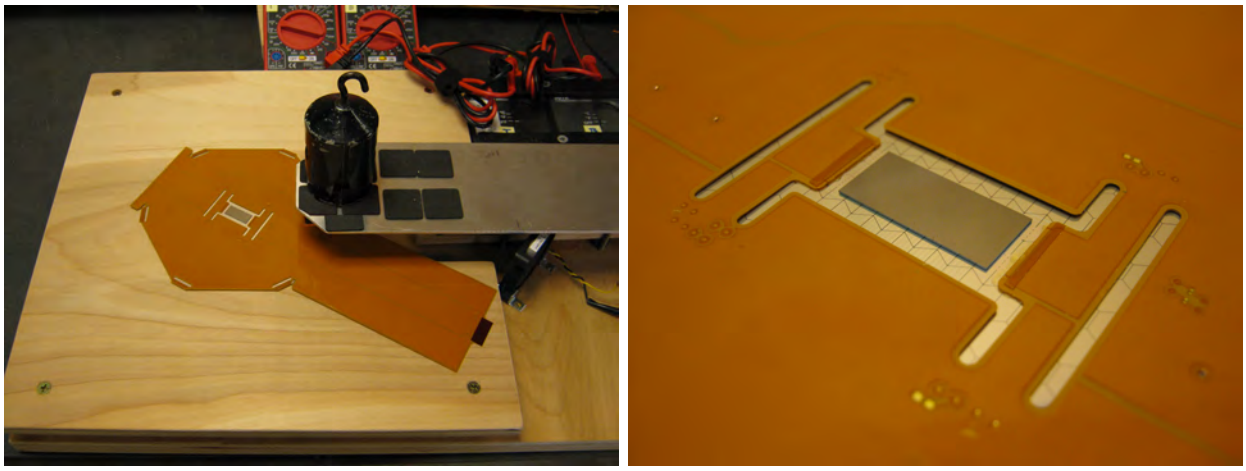

Figure 8: Left: A Photograph of the cable bonding jig that attaches the corner pads using anisotropic conductive film (ACF), and Right: a close-up photograph of the full assembly.

flow." Figure 12 illustrates two-shower separability in our event display. Initial analysis results indicate two 12 GeV electrons are separable to the diameter of two pixel diameters (about 8 mm) or less. Future work which would be highlighted in a publication will include quantitative results on shower development, comparison to simulation, and pattern recognition to extract the limitations for two-shower separation with this prototype.

The test beam data has also pointed to two technical problems to be addressed. One was the existence of "monster events," in which entire layers would light up. This was traced to a faulty gate reset in the KPiX readout chip. A second was the existence of parasitic coupling between signal traces and underlying pixels. This was a more subtle issue in the data, but is also is more difficult to address. One solution, which we hope to employ, is to shield the signal traces as part of the sensor fabrication.

4 Summary

We have successfully developed the technology to fabricate a test module which uses collider-ready silicon-tungsten technology with integrated readout. We were able to demonstrate very good performance in a test beam, consistent with the main expectations. Off course, there have been technical challenges from which we have drawn lessons. A main source of difficulty we had in implementing this technology was the incompatibility of aluminum metallization (sensor pads) and bump bonding (to the readout chip). For future sensors, we would require Au/Ni for the pads. The issue of parasitic coupling could be addressed by a modified sensor layout: We are exploring fabrication of new sensors in which the second metal layer acts as a shield between the signal traces and the sensor pixels over which they travel.

5 Publications and Public Talks Related to this Project

5.1 Refereed journal papers

1. "Gold-stud bump bonding for HEP applications," S. M. Tripathi *et al.*, JINST **5** (2010) C08005,

2. "Development of Readout Interconnections for the Si-W Calorimeter of SiD," M. Woods *et al.*, JINST **6** (2011) C12050, [arXiv:1110.6924 [physics.ins-det]].

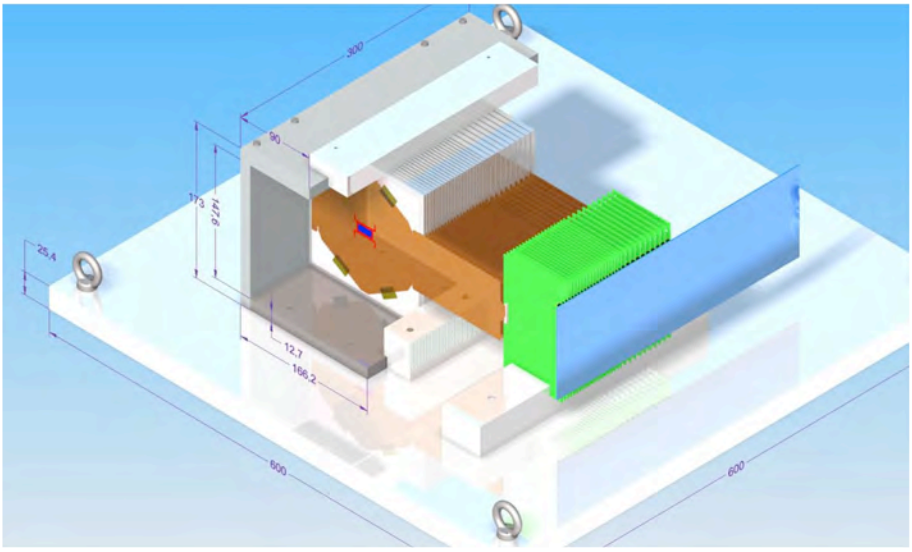

Figure 9: Schematic of silicon-tungsten ECal test module.

3. "A silicon-tungsten electromagnetic calorimeter with integrated electronics for the International Linear Collider," J. Brau, M. Breidenbach, R. Frey, D. Freytag, C. Gallagher, N. Graf, G. Haller and R. Herbst *et al.*, J. Phys. Conf. Ser. **404** (2012) 012067.

5.2 Reports and other articles

1. "International Linear Collider Physics and Detectors: 2011 Status Report", J. Brau et al. (editors), ILC-REPORT-2011-033 (2011) 109p.

2. "KPiX - A 1,024 Channel Readout ASIC for the ILC, J. Brau, M. Breidenbach, A. Dragone, G. Fields, R. Frey, D. Freytag, M. Freytag and C. Gallagher et al., IEEE Nuclear Science Symposium, DOI:10.1109/NSSMIC.2012.6551433, Published in: Nuclear Science Symposium and Medical Imaging Conference (NSS/MIC), 2012 IEEE.

3. "The International Linear Collider Technical Design Report - Volume 4: Detectors, T. Behnke et al., arXiv:1306.6329 [physics.ins-det].

5.3 Public talks

1. "Developments in Si-W Calorimeter Interconnections and Sensor Assembly," M. Woods, UC Davis, talk at ALCPG11, Eugene, Oregon, March 20, 2011, `http://agenda.linearcollider.org/event/4572/timetable`.

2. "KPiX Readout Chip Status and Application to Si-W ECal," P. Radloff (U Oregon), talk at ALCPG11, Eugene, Oregon, March 20, 2011, `http://agenda.linearcollider.org/event/4572/timetable`.

3. "Electromagnetic calorimeters at Lepton Colliders," R. Frey (Oregon), talk at Muon Collider 2011, June 2011, Telluride, CO, `http://conferences.fnal.gov/muon11/`

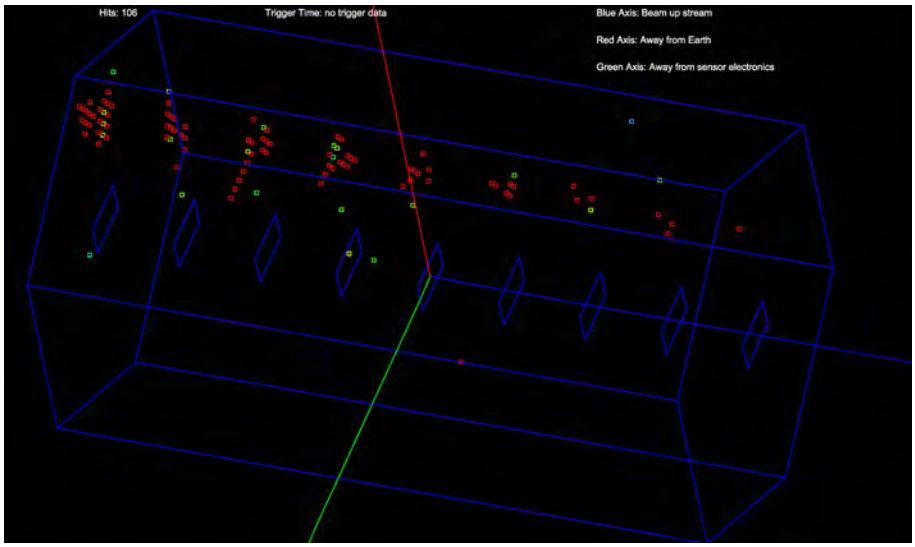

Figure 10: Typical event display of a single electron showering in the test beam prototype. separated by about one cm. The red dots indicate hit pixels. The beam direction is right to left in this view.

4. "KPiX - A 1,024 Channel Readout ASIC for the ILC, M. Breidenbach (SLAC), talk at 2012 IEEE Nuclear Science Symposium.

5. "SiD Silicon Tungsten ECAL, J. Brau (Oregon), talk at ECFA Linear Collider Workshop, DESY, May 28, 2013.

6. "Prototype Silicon-tungsten ECal with Integrated Electronics: First Look with Test Beam, J. Brau, talk at LCWS, Tokyo, November 12, 2013.

7. "A Prototype Silicon-Tungsten Calorimeter with Integrated Readout," R. Frey (Oregon), 2014 IEEE Nuclear Science Symposium, Seattle, Nov 11, 2014, `http://nssmic2014.npss-confs.org/index.php`

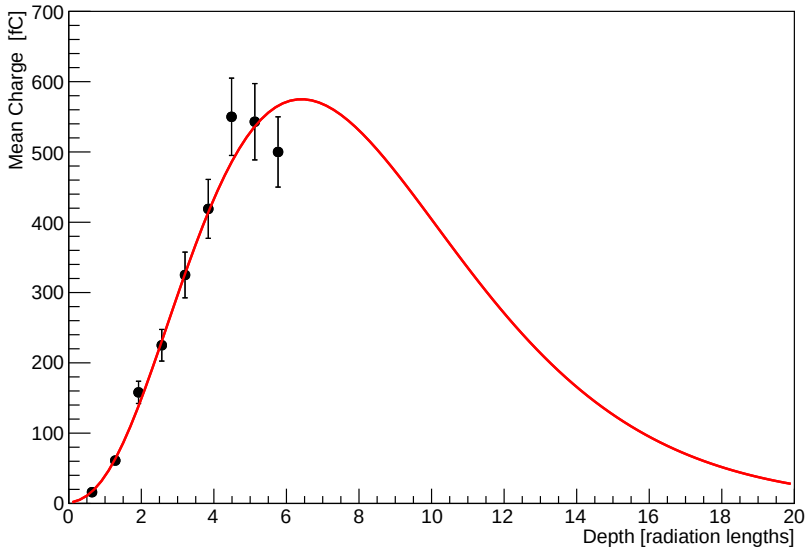

Figure 11: Total deposited energy by sensor layer. The nine layers installed for the test beam comprised about six radiation lengths.

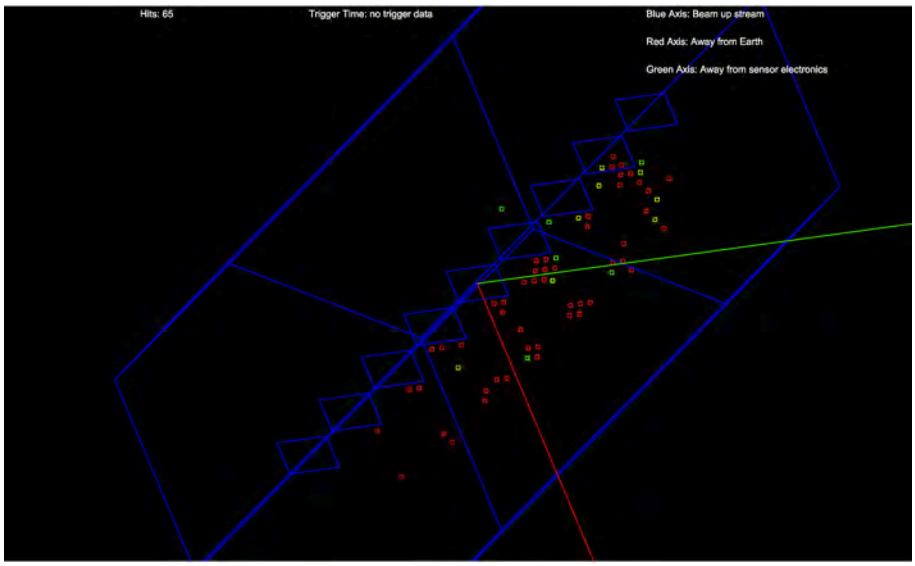

Figure 12: Event display showing two electron showers separated by about one cm. The electrons are traversing the calorimeter from lower left to upper right in the figure.

Final Report: Development of Large Area Gas Electron Multiplier Detector and Its Application to a Digital Hadron Calorimeter for Future Collider Experiments

J. Yu(PI)* and A. White*
The University of Texas at Arlington
Collaborating institutions: SLAC National Accelerator Center, Argonne National Laboratory

The UTA High Energy Physics Group conducted generic detector development based on large-area, very thin and high sensitivity gas detectors using gas electron multiplier (GEM) technology. This is in preparation for a use as a sensitive medium for sampling calorimeters in future collider experiments at the Energy Frontier. We also have been monitoring the long term behavior of one of the prototype detectors (30cmx30cm) read out by the SLAC-developed 13-bit KPiX analog chip over three years and have made presentations of results at various APS meetings. We have jointly developed 33cmx100cm large GEM foils with the CERN gas detector development group to construct 33cm x100cm unit chambers. Three of these unit chambers will be put together to form a 1m x 1m detector plane. Following characterization of one 33cmx100cm unit chamber prototype, a total of five 1m x 1m planes will be constructed and inserted into an existing $1m^3$ RPC DHCAL stack to test the performance of the new GEM DHCAL in particle beams.

The large area GEM detector we planned to develop in this proposal not only gives an important option to DHCAL for future collider experiments but also has the potential to expand its use to Intensity Frontier and Cosmic Frontier experiments as high efficiency, high amplification anode planes for liquid Argon time projection chambers. Finally, thanks to its sensitivity to X-rays and other neutral radiations and its light-weight characteristics, the large area GEM has a great potential for the use in medical imaging and homeland security, as well as satellite based astronomy experiments.

Long term behavior of GEM

As part of the study for GEM detector development, we have been monitoring the long term response of a 30cmx30cm prototype, using cosmic rays. The detector has been read out with KPiX. Fig. 1.(a) below shows the gain as a function of ambient pressure, $G = -303.9\,p(KPcal) + 33509$. A pressure correction factor has been obtained by normalizing the gain $f = G(1atm)/G(P)$ to compensate the pressure variation of the chamber gain due to the open gas system configuration of the prototype detector system. Figure 1.(b) shows a typical pressure corrected charge distribution of the chamber to the cosmic muons. Figure 1.(c) shows the chamber response measured by the fit results of the MPV from each of the cosmic runs. Orange data points are pressure corrected responses, while the blue line is the response before the correction. Figure 1.(d) shows a 1D histogram of fit MPV and demonstrates the stability of the chamber responses. This result has been presented at the APS April meeting, Texas Section APS meetings, and to WoPhyS in 2013 by Yvonne Ng, one of our female undergraduate research assistants.

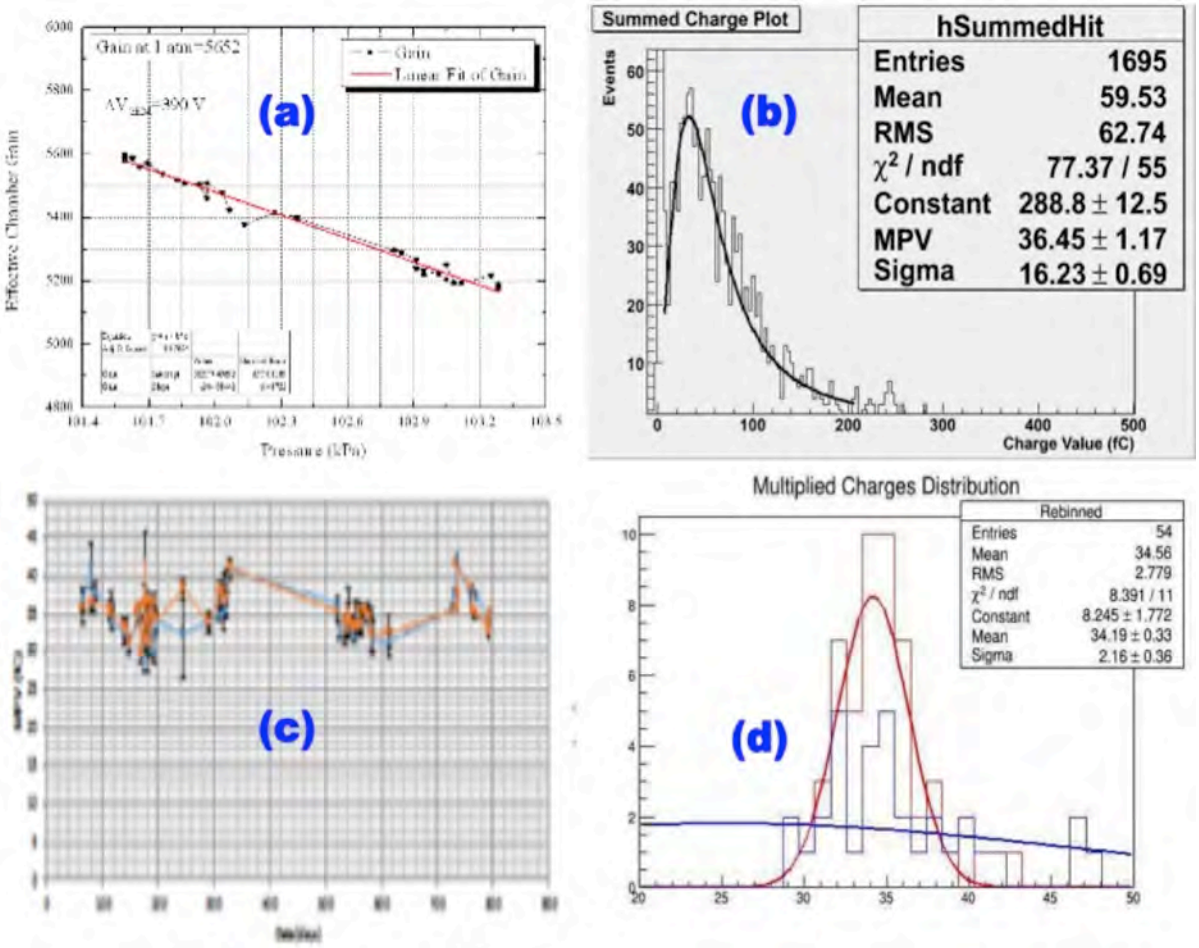

Figure. 1 (a) Gain as a function of the ambient pressure used to correct pressure variations (b) A typical pressure corrected MIP charge distribution of a cosmic run (c) Measured gain vs date monitored for about 900 days with (orange) and without (blue) the pressure correction (d) 1D distribution of MPV values for several cosmic ray runs, demonstrating the stability of the chamber response for about 3 years.

Large GEM Development for DHCAL

Since the area of the new GEM foils is much larger than any of the GEM foils we have used to construct prototypes previously, they could be contaminated by dirt or other objects that might get into the holes. Thus, as the first step in constructing a large area $33\text{cm} \times 100\text{cm}$ unit chambers, we built a 12'x8' class 10,000 clean room as shown in Fig.2(a). We then proceed to construct two unit chambers using the four LGEM foils that pass the qualification criteria. Figure 2.(b) shows a layer of a prototype chamber with G-10 spacer being glued on a GEM foil. The twelve alignment pins are holding parts on an aluminum jig plate. Figure 2.(c) shows a snap shot taken during a glue curing process with a heavy pressing plane to hold parts together flat. We are very close to completing a unit chamber, excluding the anode layer. Figure 2.(d) shows our design of 100cmx100cm chamber for a beam test in CALICE calorimeter stack. While we have been in discussion with the SLAC KPiX team to make a 32cm x96 cm anode board to read

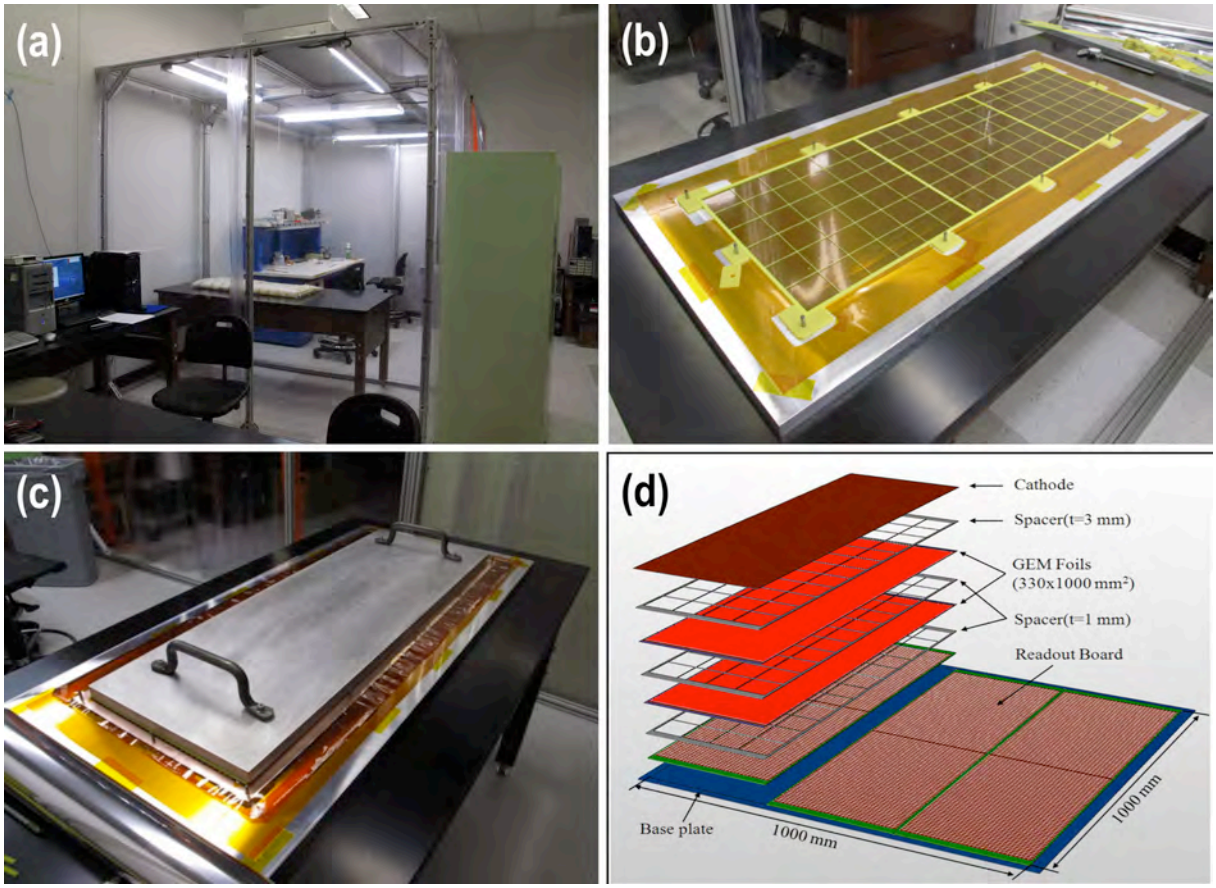

Figure. 2 (a) 12'x8' clean room for LGEM construction (b) An LGEM layer on an assembly jig held by alignment pins throughout the sides (c) glue curing process with heavy flattening pressing plane (d) Layout of a full $100\text{cm} \times 100\text{cm}$ **GEM DHCAL active layer.**

out the large area; however due to the lack of funding on SLAC team, the readout board was not yet produced. Thus, our large chambers are at the moment without the readout boards.

Conclusions

The UTA HEP group has been monitoring the long term stability of a 30cmx30cm prototype GEM chamber. Due to the shortage of the funds, we could not complete the development of large GEM chambers for the digital hadron calorimeter application We hope that the funding situation improves for the development of ILC detectors so that our expertise in large GEM chamber puts our group in a strategic position to take full advantage of the opportunity to provide a solution to the calorimetry needs such a detector.

Lepton Collider Detector R&D

New Materials and Gases for Resistive Plate Chambers for Hcal and Muon Systems in a Lepton Collider Detector

Final Report

Personnel and Institution(s)

Changguo Lu, Kirk T. McDonald, William R. Sands, A. J. S. Smith,
Princeton University

Collaborators

New material development, Jiawen Zhang, IHEP, Beijing, China,
Mingfa Su, Xianhu, Inc. Beijing (Beijing Kadesh Boild Materials Co. Ltd), China

Project Leader

Name: Kirk T. McDonald
Email: kirkmcd@princeton.edu
Phone: 609-258-6608; cell: 609-933-6601

Project Description

This project was a continuation of effort begun as part of SiD detector R&D, to study and develop mitigations to the phenomenon of aging of the electrodes of resistive plate chambers (RPCs). These devices are leading candidates for low-cost tracking detectors for particles in muon systems, and hadron calorimeters of future lepton collider detectors. However, the present need to operate these detectors with gas mixtures that include fluorine (to suppress fluctuations in the gas-amplification process initiated by passing high-energy charged particles) leads to the formation of HF acid which can attach the detector electrodes with eventual loss of performance.

This effort grew out of studies of the aging of the BaBar drift chamber.[1]

In the SiD R&D project we investigated aging phenomena in BESIII-type RPCs, with results published in two papers,[2,3] and a third internal note.[4] Also, we procured

---

[1] C. Lu, *BaBar drift chamber aging study*, NIM A **518**, 125 (2004).
[2] C. Lu, *RPC electrode material study*, NIM A **602**, 761 (2009).
[3] C. Lu *et al*., *Aging Study for the BESIII-type RPC*, NIM A **661**, S226 (2012).
[4] C. Lu *et al,. Microscope study of BESIII-Type RPC Aging Phenomena* (Sept. 8, 2010), http://puhep1.princeton.edu/~mcdonald/ILC/MicroscopeStudyOfAging.pdf

initial samples of Bakelite treated with a linseed-oil-impregnated resin (from Xianhu, Inc.)[5] and begun study of RPCs constructed from these.

The present LCD R&D proposal will continue and extend our efforts to produce age-resistant RPCs via three approaches:

1) Modify the surface material of the electrode to make it HF resistant. This is the path we have explored to date, with some preliminary success. We have found a possible HF resistant resin, which can be used to coat Bakelite sheets.
2) Search for alternative gas mixtures that do not incorporate fluorine atoms, which are the source of HF in the gas avalanche.

2.1 Modified Bakelite materials

Unfortunately, the various new samples of modified Bakelite that we obtained from a company (Xianhu, Inc.) in Beijing, China did not show the improvement we had hoped for, and the search for better Bakelite materials has been discontinued.

2.2 Freon-less gas mixture

We have explored one Freon-less gas mixtures for streamer mode RPCs: Ar/CO_2/Isobutane/SF_6 (31/60/8/1). We used the same RPCs as previously subject to aging tests, so their efficiency was not high. Preliminary efficiency plateaus for 5 test chambers are shown in Figure 1.

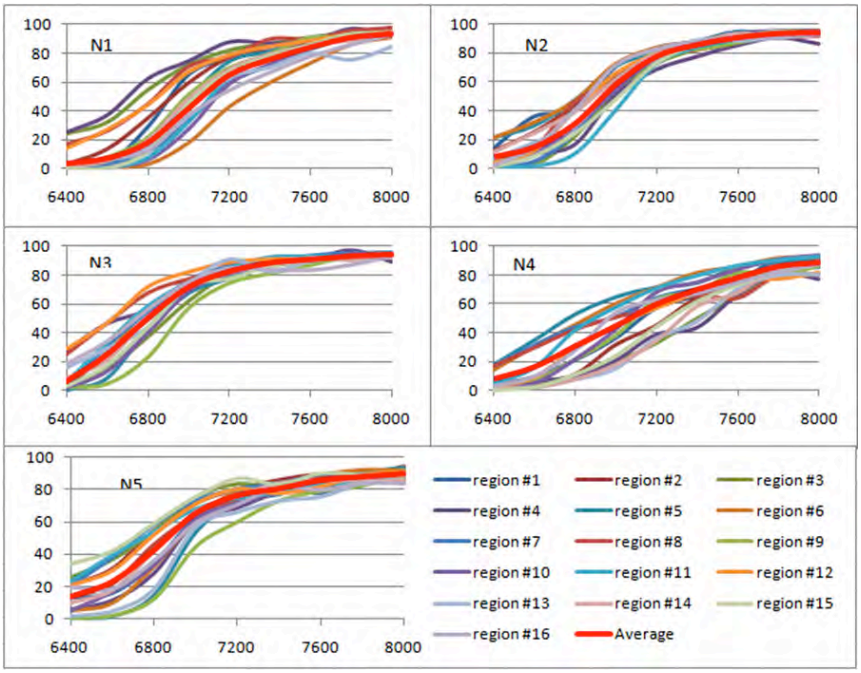

Figure 1. Efficiency plateaus in 5 previously aged RPCS (N1-5) with a Freon-less gas mixture.

[5] J. Zhang *et al., A new surface treatment for the prototype RPCs of the BESIII spectrometer*, NIM A **540**, 102 (2005).

For comparison, the efficiency plateaus of these 5 RPCS when operated (after aging) with our nominal RPC gas mixture Ar/R134A/Isobutane/SF6 (65.5/30/4/0.5) are shown in Fig. 2.

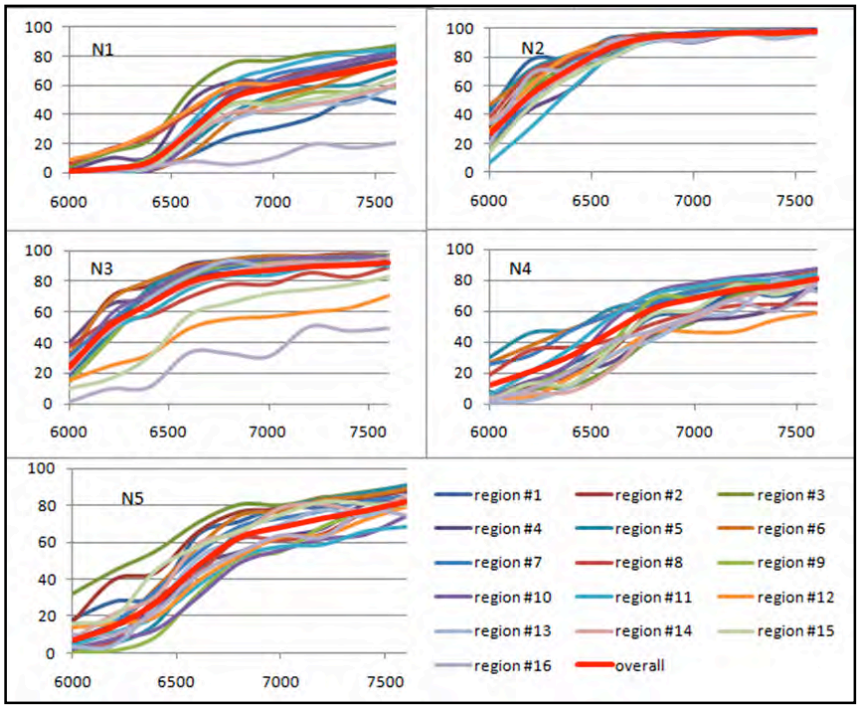

Figure 2. Efficiency plateaus in 5 previously aged RPCS (N1-5) with a Freon gas mixture.

Due to the prior aging these plateaus were not great, but an interesting observation is these very bad regions of RPCs N1 and N3 seen in Fig. 2 do not exist anymore. The high voltage of the overall efficiency plateaus was shifted up ~ 400 V. It seemed like these RPCs had "forgotten" the aging damage, a phenomenon deserving further study.

More detailed characterization of the RPC signals showed that the streamer charge spectrum in the Freon-less gas mixture was much broader, and the streamer multiplicity was also higher, than with the Freon-based mixture. These are good features for use of RPCs in a hadron calorimeter, so further searches for better gas mixtures are needed.

DHCAL Progress Report

1. Construction and Assembly of the Large DHCAL Physics Prototype

In order to validate the Digital Hadron Calorimeter (DHCAL) concept, gain experience running large Resistive Plate Chamber (RPC) systems and measure hadronic showers in great detail as well as validate the hadronic shower models, a large prototype section of 38 layers and a tail catcher section with 13 layers were constructed. The total readout channel count is close to 470000. Each layer consists of 3 RPCs of size 32 x 96 cm^2. Readout is performed with 1 x 1 cm^2 pads with one threshold (1-bit), hence digital calorimeter.

1.1.RPC Construction

This step consists of a difficult resistive paint spraying procedure on the RPC glass surface (Fig. 1). RMS of the resistivity is taken as a measure for quality checks. RPC assembly is also very labor intensive. Overall quality of the assembly is very good and more than 90% of the RPCs were accepted.

Figure 1. Resistive paint spraying stand.

Figure 2. Assembled RPCs.

1.2.RPC Tests

All RPCs passed the leak test at 0.30" water pressure. High voltage (HV) tests were performed in a cassette-like environment. Typical dark current was measured to be ~0.25μA/chamber. RPC are then tested with cosmic rays.

1.3.Front-End Boards

Each board contains 1536 channels and 24 ASICs. The data concentrator is implemented into the same board. 2 boards are needed per RPC. We built three computer controlled test stations to perform extensive tests (S-curves, noise rates…). Accepted boards with less than 4/1536 dead channels.

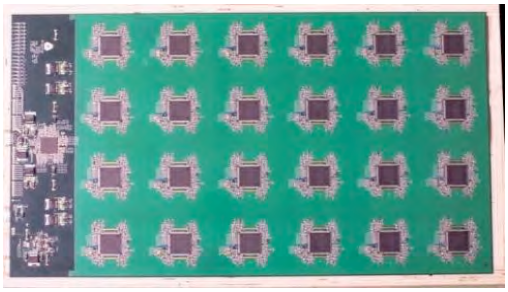

Figure 3. Front-end board.

1.4 Pad and Front-End Board Gluing

Each board contains 1536 channels which need to be connected with conductive glue. The glue dries in 3 hours. We built a gluing fixture. Dispensing of the glue on gluing dots takes 25 minutes per board. We glued 10 boards per day and the glue is cured in oven at 70 ^{o}C.

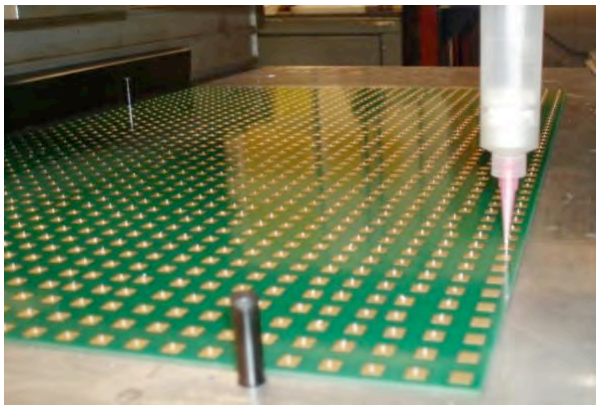

Figure 4. Gluing fixture.

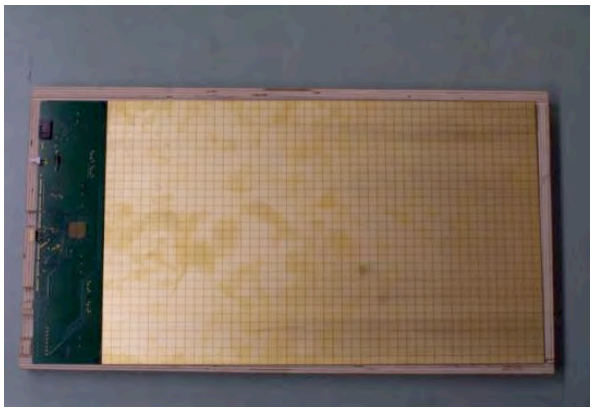

Figure 5. Pad and front-end board after gluing.

1.5 Data Collector and Timing and Triggering Modules

1 Data Collector Module (DCOL) per 12 front-end boards is required. Modules were tested at Boston and delivered to Argonne. Timing and triggering modules (TTM) provide control to up to 24 Data Collectors. 1 Master and 2 Slave modules were used. These modules were designed and debugged at Fermilab.

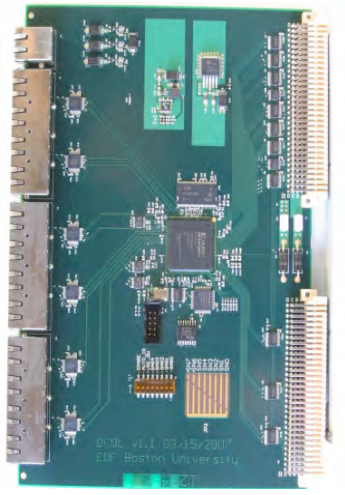

Figure 6. DCOL.

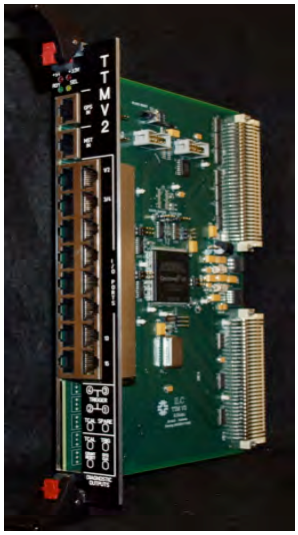

Figure 7. TTM.

1.6 Cassette Assembly

3 RPCs are assembled into a cassette. Front-plate is copper (for cooling of ASICs) and back plane is steel. Cassette is compressed horizontally with a set of 4 (Badminton) strings. Strings are

tensioned to ~ 20 lbs. Cassettes were tested with cosmic rays.

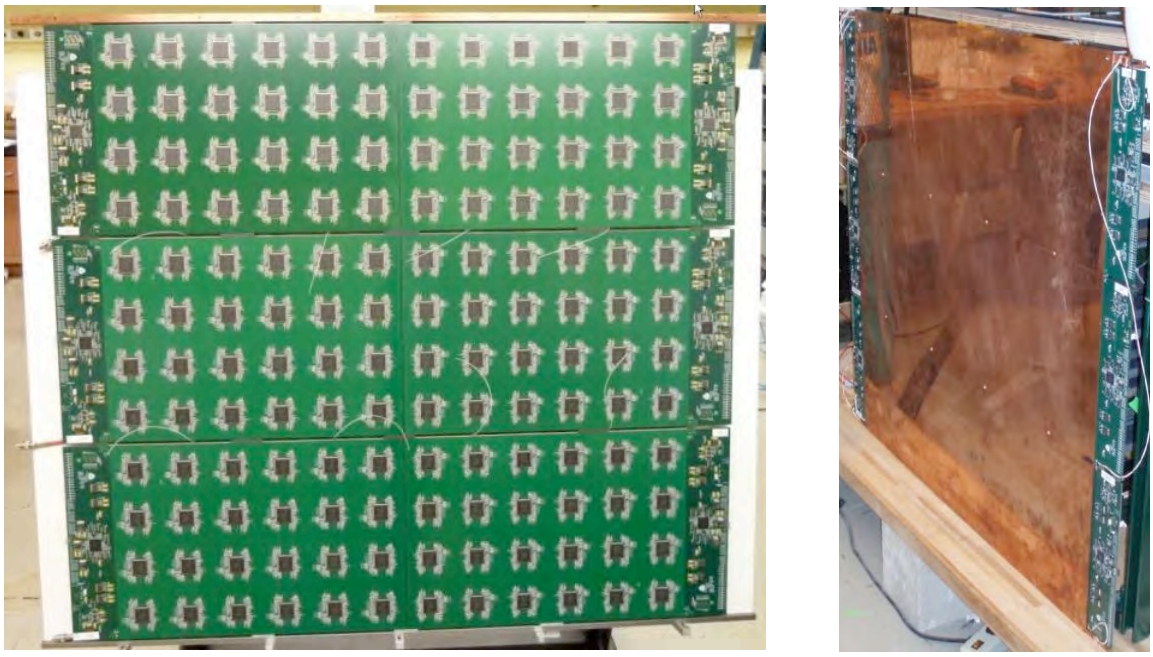

(a) **(b)**

Figure 8. Front-end boards, spacers and the ends of badminton strings as seen in the cassette frame (a) and a fully assembled cassette (b).

1.7.Peripherals

1.7.1. Low Voltage Power Supply

306 front-end boards were powered at +5V. We acquired 7 Wiener power supplies and built 7 power distribution boxes.

1.7.2. High Voltage Power Supply

Three RPCs were powered by one line. We used four partially filled LeCroy 4032 power supplies and a computer control program with CAMAC to USB interface. We had to use Droege power supplies for part of the tail catcher layers due to insufficient number of LeCroy channels that were able to survive until the end of the beam tests.

1.7.3. Gas Supply

One gas line is required for two layers (or 6 RPCs). We built a mixing rack for three gases and a distribution rack.



(a) (b) (c)

Figure 9. Low voltage rack (a), gas mixing rack (b) and the high voltage rack (c).

2. Beam Tests

We successfully completed the below test beam program:

- October 2010 – November 2011: Fermilab Test Beam Facility, CALICE steel absorber structure Fe-DHCAL, 1 - 120 GeV, 9.4M muon events, 14.3M secondary beam events.
- May 2012: CERN PS, CERN tungsten absorber structure W-DHCAL, 1 – 10 GeV.
- June – November 2012: CERN SPS, CERN tungsten absorber structure W-DHCAL, 10 – 180 GeV, CERN TB total 4.9M muon events, 22.1M secondary beam events.

Figure 10 shows the test setups at FTBF (top) and CERN (bottom) beam tests.

Figure 10. Beam test setup in FTBF (top) and CERN (bottom).

Figure 11 shows event displays of a muon (a) a pion (b) and a positron (c) in the DHCAL.

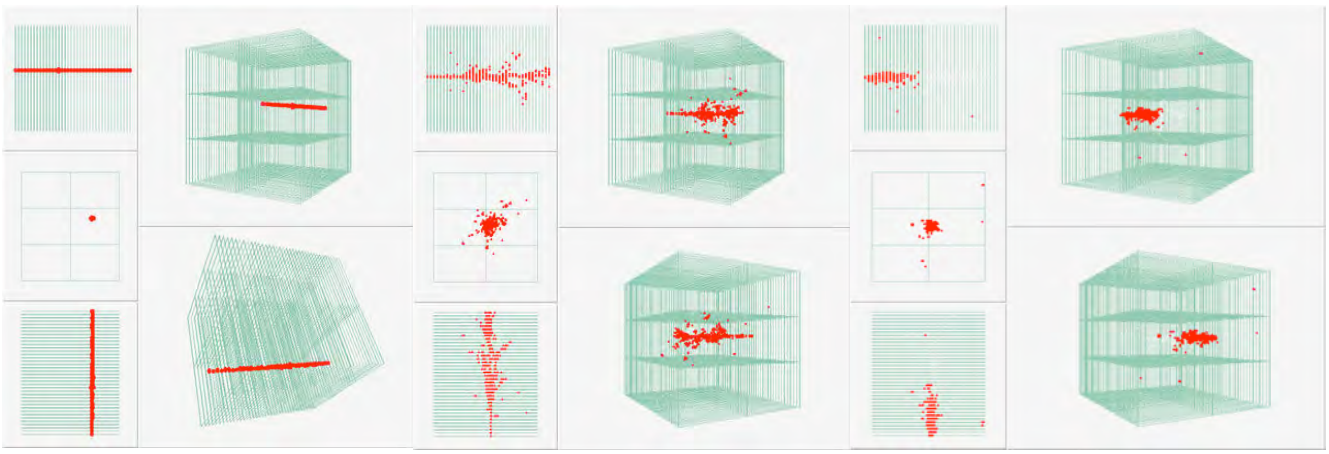

(a) **(b)** **(c)**

Figure 11. Muons (a), pions (b) and positrons (c) in DHCAL.

Figure 12 shows the response of the Fe-DHCAL to hadrons. The response non-linearity is around 2-4% and the hadron energy resolution is around 65%.

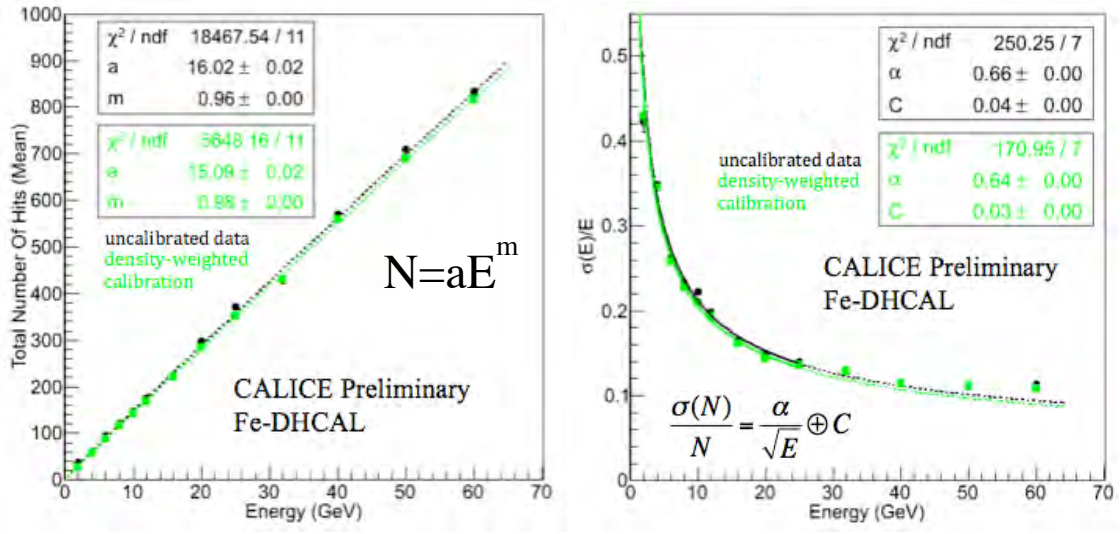

Figure 12. Response of the DHCAL to pions (left) and the hadronic energy resolution (right). Results are from the Fermilab test beam data analysis both for uncalibrated data (black) and after applying density-weighted calibration (green). The calibration scheme improves both the linearity and the resolution. For details of the analysis see CAN-042 [9].

The group at University of Iowa pursued below developments for the possibility of large-scale, RPC-based Digital Hadron Calorimeters for collider experiments:

a) Development of a gas recycling facility

For cost reasons and to protect the environment (from green house gases), the gas used by larger RPC systems must be recycled. We propose to develop a new recirculation system, dubbed 'Zero Pressure Containment'.

A recirculation system is a semi-automatic feedback control loop coupled with an analysis/quality control system. Building such a system and getting it to work in a stable equilibrium is a challenge. There are three main "new" aspects to this system. The first is the purification process, which will involve several types of molecular sieves, activated alumina/copper, activated carbon, and particulate filters (coupled with compressors, regulators). The second is the analysis part, which might include atmospheric analysis, electronegative characterization, possible use of a "canary" chamber, and other more sophisticated tools (gas chromatograph). The third "new" aspect is the manifold of the detectors, which will look very different from what is being used presently.

The manifold of the input and output lines need to be designed in such a way as to maintain a constant pressure difference between the input and output sides. The corrosivity of the exhaust gas makes copper undesirable for long-term use. Therefore, much of the system will need to be made of stainless steel. This system does not include any electronic flow controls, which might be necessary. Iowa will provide a mass spectrograph type of gas analyzer. The conceptual design including the gas mixing system is shown in Fig. 13.

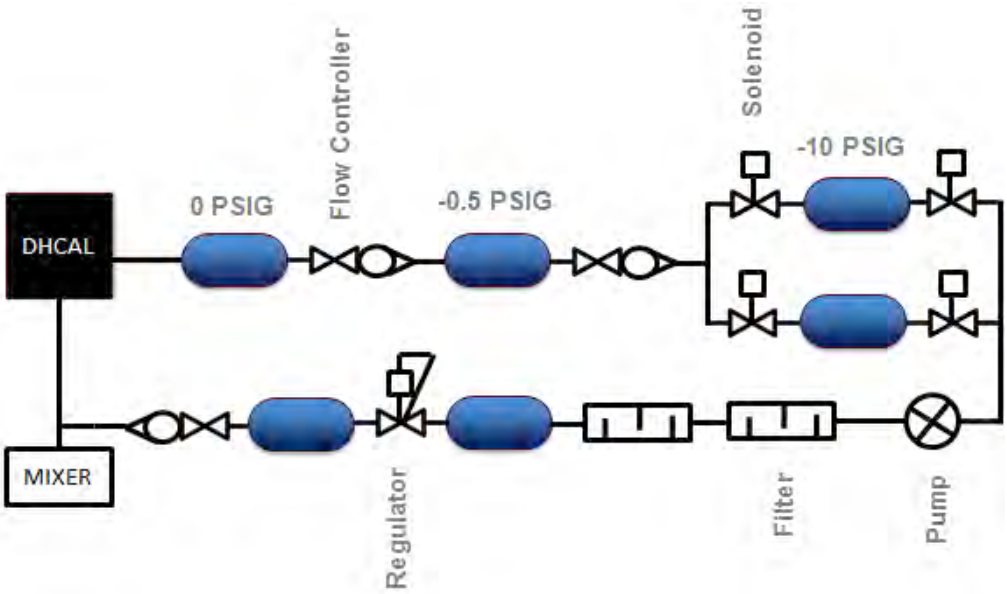

Figure 13. Schematic of the gas recirculation system.

This R&D was stalled at the stage of minor partial assembly due to lack of funding.

b) Development of a high voltage generation and distribution system

The technical prototype module consists of 54 active layers. The approach taken for the prototype section to supply each chamber individually with high voltage is not a viable solution for larger-scale systems. A system consisting of a single power supply per module together with a distribution system to the layers needs to be developed. The possibilities of adjusting the voltage and monitoring the currents for each layer are necessary. A system based on the Cockcroft-Walton technology is being considered.

A small-scale prototype was designed and built at the University of Iowa, and was successfully tested with RPCs at Argonne National Laboratory. The R&D was stalled at this stage due to lack of funding. The building and tests of a larger prototype were not performed. When this second stage is successfully completed, such systems can be useful for any current or future calorimeter in need of a large number of high voltage channels.

c) Development of low resistivity glass

The purpose of this R&D is to develop low resistivity glass with the optimum resistivity to allow larger counting rates but still have the desirable RPC performance. The recent developments by the COE College show that resistivities at the order of 10^7 and 10^3 Ω/cm^2 can be acquired with iron and copper doped lead vanadates. Several sets of low-resistivity glass were produced and the RPCs constructed with this glass were tested at Fermilab. The results clearly indicate that the tuning of the resistivity is under control and the RPC performance progresses as expected. This part of the R&D was performed completely by other sources of funding.

d) Contribution to the development of a data analysis frame work

The funding allowed only ½ FTE for the analysis effort. Given the novelty of the data and the richness of possible calorimetry techniques that can be developed, this effort was not sufficient for the full production.

References

[1] L. Xia, Proceedings of the XII International Conference on Calorimetry in High Energy Physics, Chicago, AIP Conf.Proc. **867**: 531-537, 2006.

[2] J.Repond, Proceedings of the 10th Pisa Meeting on Advanced Detectors, la Biodola, Isola d'Elba, Italy, Nucl. Instr. Meth. **A572**, 211(2007).

[3] G.Drake et al., "Resistive Plate Chambers for hadron calorimetry: Tests with analog readout", Nucl. Instrum. Meth, **A578**, 88-97 (2007).

[4] B. Bilki et.al., "Calibration of a digital hadron calorimeter with muons", JINST 3 P05001, 2008.

[5] B. Bilki et.al., "Measurement of the rate capability of Resistive Plate Chambers", JINST 4 P06003, 2009.

[6] B. Bilki et.al., "Measurement of positron showers with a digital hadron calorimeter", JINST 4 P04006, 2009.

[7] B. Bilki et.al., "Hadron showers in a digital hadron calorimeter", JINST 4 P10008, 2009.

[8] Q. Zhang et.al., "Environmental dependence of the performance of resistive plate chambers", JINST 5 P02007, 2010.

[9] https://twiki.cern.ch/twiki/bin/view/CALICE/CaliceAnalysisNotes : CAN-030 Analysis of DHCAL Muon Data; CAN-031 DHCAL Noise Analysis; CAN-032 DHCAL Response to Positrons and Pions; CAN-039 Analysis of Tungsten-DHCAL Data from CERN Test Beam; CAN-042 The DHCAL Results from Fermilab Beam Tests: Calibration.

[10] https://silicondetector.org/display/SiD/home .

[11] http://clic-study.org/ .

Progress Report on Improving the SiD Particle Flow Algorithm from the University of Iowa

Usha Mallik

1 Introduction

The University of Iowa group under the leadership of Usha Mallik developed a generic Particle Flow Algorithm (PFA) for the Letter-of-Intent (LOI) for the International Linear Collider (ILC) SiD concept; this was used for the validation of SiD by the International Detector Advisory group (IDAG) in 2009. While several university and laboratory groups contributed to establishing a PFA effort in the U.S., The University of Iowa has been the primary contributor to this effort in collaboration with SLAC in the five years from 2007 till 2012.

Particle Flow Algorithms (PFAs) are the recognized tool to achieve the desired resolution for detectors at high energy future lepton colliders, of which the International linear collider (ILC) and the compact linear collider (CLIC) are under consideration. Some aspects of a PFA were used in some of the LEP and the Tevatron detectors once the experiments were mature; the Compact Muon Solenoid (CMS) detector at the LHC also uses some of the principles of a PFA.

The original PFA used to achieve the physics benchmarks for the SiD concept at 500 GeV e^+e^- center-of-mass (CM) energy was the work of Matthew Charles, an Assistant Research Scientist from the Iowa group, and Usha Mallik in collaboration with SLAC[1].

The next goal of the Iowa PFA was to improve the overall performance at 500 GeV and at higher collider energies (e.g. CLIC) in both resolution and in CPU consumption for the Detailed Baseline Design (DBD) scheduled for late 2012, specifically up to 1 TeV center-of-mass energy. This was accomplished by Remi Zaidan, a postdoc who joined Iowa in late 2009 and Garabed Halladjian, who joined in late 2010, expressly to work on the PFA. Mat left in late 2008 to take up a position at Oxford. Remi started to learn the PFA algorithm with help from Mat and at times from Ron Cassell (SLAC). By late 2010 he developed enough expertise to help initiate Garabed into the Iowa PFA; together they managed to achieve a substantial improvement both in performance and in CPU useage before the Detailed Baseline Design (DBD) for 500 GeV and 1 TeV cm energy.

The LOI PFA (2009) was completed with meager resources and was result-oriented against an impending deadline. Optimized for energies up to 500 GeV the event energy resolution achieved for qqbar at 500 GeV was 3.5%, and 6.3% at 1 TeV. The corresponding resolution delivered for the DBD in April 2012 is 3.1% at 500 GeV and 5.5% at 1 TeV. These were obtained with SiD02 geometry. With a realistic geomtry including all the cracks and overlaps in the corners (SiD03) a resolution worsening of $\sim$10% was observed by Ron Cassell and confirmed by our results.

[1] primarily Ronald Cassell, now deceased

2 Essential Components of the PFA

A description of the essentials of the PFA implementation is given here. The calorimeter hits are digitized and stored. Then electromagnetic interactions with electrons and photons are isolated by identifying electromagnetic clusters in the Electromagnetic Calorimeter (ECAL). If a reconstructed track extrapolated to the ECAL has a momentum matching that of a nearby EM cluster energy, it is flagged as an electron, otherwise the cluster is flagged as a photon. Muons are tracked through the ECAL, the Hadronic Calorimeter (HCAL) and the muon detector. These hits, once identified, are taken out of the list of calorimeter hits to be used for hadronic shower building. The corresponding tracks are also flagged against further use.

A modified Directed Tree algorithm (DTree) is next applied to the calorimeter hit collection which uses hit density gradient to isolate various shower cores in ECAL, HCAL and Muon detector for barrel and endcap regions. The large DTree clusters are then broken into smaller sub-clusters and a list of these pieces is prepared. These sub-clusters falls into the categories of *clump*s, *MIP*s, *block*s and *leftover* hits depending on the grouping of the hits.

Next, starting from the lowest momentum track, a seed is formed from the hits in the early ECAL layers for each charged track extrapolated to the ECAL inner boundary. The seed is then extended outward adding *clump*s, *MIP*s and *block*s using a likelihood derived from the Probability Density Functions (PDF). The PDFs are generated by training on Monte Carlo (MC) truth as a function of several geometric and kinematic variables as part of a calibration procedure. The likelihood represents the probability of any two sub-clusters to be connected according to their geometric proximity, energy distribution and shape.

During the shower reconstruction, at each step the total energy of the shower is compared with the momentum of the specific track within a tolerance (σ). Once satisfied or when there are no further well-connected clusters available, the next track in ascending order of momentum is selected and the corresponding shower is developed. When all the tracks are thus completed, the energy of the leftover hits is divided up between the neighboring clusters. A redistribution of the shower pieces is performed by looping over all of the tracks as necessary. Special cases of overlaps and division of shower energies are arbitrated in a manner suitable to the specific instance.

The four-vectors of the charged hadrons are then written out assuming a pion mass. The leftover shower pieces are then attributed to the neutral hadrons, with a K_L mass assumed for the long lived neutral hadron four-vectors.

2.1 Performance at the 2009 LOI and Leakage study

The PFA resolution achieved was good enough to obtain compatible physics performance with the ILD concept for the physics processes requested by the IDAG in 2009 for the LOI for concept validation. Because the compact nature of the SiD02 concept (HCAL 4λ compared to 6λ of the ILD), and leakage can degrade the PFA performance, we tested if leakage was indeed an issue. The upshot of the tests were that leakage indeed played a significant role, but the algorithm also could improve. This was not a surprise.

2.2 Study of Algorithmic Components

The interdependencies of the modules made the overall improvement more challenging. Some of the tools were specifically targeted for a single purpose and some were generic. Remi and Garabed together deconstructed the overall algorithm into its many interdependent modules, and

studied each module independently. It was imperative to develop appropriate diagnostic tools to determine the performance and the effect of the subsequent changes quantitatively for any one module. Each module, i.e., each piece of the PFA was studied with events at various stages of reconstruction. Since the complete PFA is the end product of many interdependent algorithmic parts, diagnostic tools were developed for each piece of algorithm independently as well as its interaction with other pieces of algorithms downstream. Specifically, the following pieces were studied which needed modification.

- MIP finding and extrapolation; an example is extrapolation of the *MIP*s across boundaries between different detector regions, like the barrel and endcap, which split apart DTree clusters
- photon finding efficiency: hits from the photons once identified are vetoed from the list of hits; lower efficiency means we have extra non-hadron hits for later cluster formation;
- division into *clump*s, *block*s and *leftover* hits following the DTree clustering: sub-cluster sizes needed to be optimized with improved purity, too many left-over hits were observed;
- the PDFs needed updating; those generated at lower jet energy, where isolation of showers was relatively easy, was being used at higher energies with substantial shower overlaps;
- at higher energies overlap of the showers of multiple tracks makes the reconstruction challenging;
- the need for a more sophisticated global algorithm of shower reconstruction for all of the tracks instead of one track at a time; in the first pass the skeleton of the shower cores with high purity would be found for all of the tracks one at a time, to be followed by a second pass with arbitration of the additional shower pieces between different tracks;
- the shower reconstruction algorithm itself was studied in detail and was thoroughly modified.

3 Progress since the LOI

We formed a plan to improve the existing PFA implementation. The plan, and the step-by-step progress made, is described below. 1) MIP algorithms: At several places in the PFA pieces of MIPs are established, extended, interpolated or matched. The specific algorithm depends on the purpose and where in the overall PFA it is used.

a) In seed finding a reconstructed charged hadron track is extrapolated to the inner face of the ECAL and a MIP-like piece in the early layers of the ECAL, if present, is matched with the track as a seed. This was improved with the addition of directional information. It was also modified to run much faster.

b) In the SiD geometry MIPs crossing the ECAL barrel into the HCAL endcap enter at a steep angle. These special cases were not treated properly previously and the efficiency of MIP extension across the boundary was lower. This has now been corrected.

c) In cases where hits in intermediate layers were missing, the extrapolation behaved incorrectly when certain specific conditions were met, and lowered the efficiency. This has now been fixed.

Section	energy-weighted purity *clump*s: baseline	energy-weighted purity for *clump*s: current	energy fraction *clump*s: baseline	energy fraction *clump*s: current
ECAL	90%	94%	15.3%	16.2%
HCAL	80%	87%	32.2%	29.0%
Overall	84%	90%	47.5%	45.2%

Table 1: Energy-weighted purity of the *clump* sub-cluster types, from baseline and with the current improved DTree sub-clustering. A significant improvement in purity is observed in the HCAL. Purity is calculated by comparing the sub-clusters from the MC truth with those formed by the modified DTree algorithm.

2) Improvement in photon-finding efficiency: The effect of efficiency and purity on the shower reconstruction was studied. At the Oregon SiD workshop Zaidan showed[2] a comparison of the PFA performance with the current photon reconstruction and with the *cheat photon finding* (MC truth), finding much better overall resolution with the latter. (Originally Ron Cassell worked on it.)

3)Cluster Purity: The majority of sub-clusters from the modified DTree are *clump*s and *MIP*s with quite a few leftovers. In general *clump*s are dense clump of a large number of localized hits, *MIP*s are MIP-like fragments through the calorimeter, and *block*s are a number of grouped hits without a dense core like that in a *clump*, but a localized group of a few hits nevertheless. We studied the effect of the *clump*s, and observed that purity of the HCAL clumps was substandard, and needed to be improved substantially. The subclustering in DTree was then modified with improved purity and currently the energy-weighted averages of the clumps, blocks, MIPs and leftovers are listed in Table 1 where the corresponding numbers from the baseline (2009 LOI) are also shown. A substantial improvement, especially in the HCAL, is evident.

4)Likelihood: For optimal performance the PDFs used for likelihood calculation should describe the distributions in the event to be reconstructed as closely as possible. In the 2009 baseline a trial pre-DTree clustering was used to generate the PDFs which was different from the clustering used in shower reconstruction. As the PFA was tuned for lower energies where the showers were comparatively isolated, this made little difference in the final performance. However, at higher energies, the situation is a lot more complex and now consistent PDFs at the proper energy are being used for generating the PDFs as well as in shower building. In addition, other variables are added to the likelihood to improve its discrimination.

5) Shower Reconstruction: In connecting the *clumps/MIPs/blocks*, the likelihood method applied is improved using new information taking correlations into account. Various geometric variables such as angles, Distance of Closest Approach (DOCA), etc. are used. The exact variable list used depends on which two sub-cluster types are (*clump*s, *MIP*s or *block*s) being considered, and which variables have sufficient discrimination power to form a good likelihood criterion. These variables are illustrated in Fig 1. The effect of using these angles b and c are shown in Figs. 2 (a) and (b) in the likelihood functions, and in Fig 3 as the rejection power vs efficiency, for all types of sub-cluster pairs together.

Because of limited statistics, we do not use a full multi-dimensional likelihood. Instead, several two-dimensional PDFs are applied to take the correlations into account. The correlations between different pieces of a shower (like clump-clump) where both belonged to the same shower cluster and when they did not were studied from the signal and the background samples.

[2] http://ilcagenda.linearcollider.org/getFile.py/access?contribId=9&sessionId=3&resId=0&materialId=slides&confId=4766

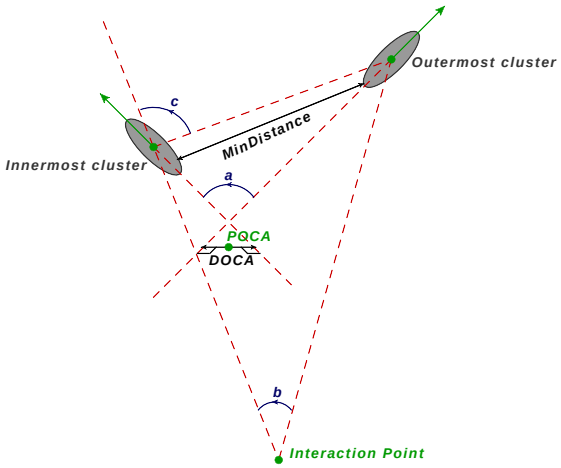

Figure 1: The discriminating variables used in the likelihood to determine whether a pair of sub-clusters belong to the same shower or not. Different combinations of the variables are used for different types of sub-cluster pairs.

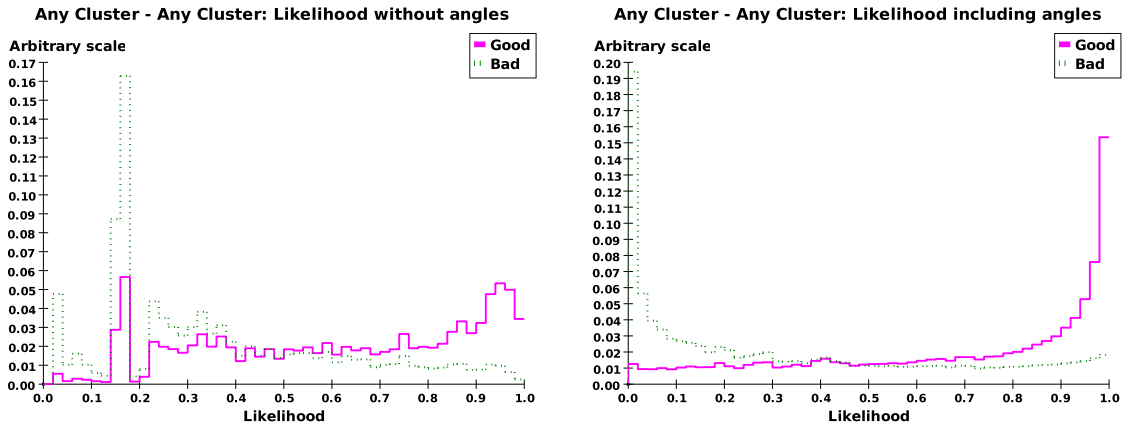

Figure 2: The discriminating power of the angles. The likelihood discrimination is shown without (left) and with (right) use of the angles b and c pairs of sub-clusters that come from the same shower (good) or different showers (bad).

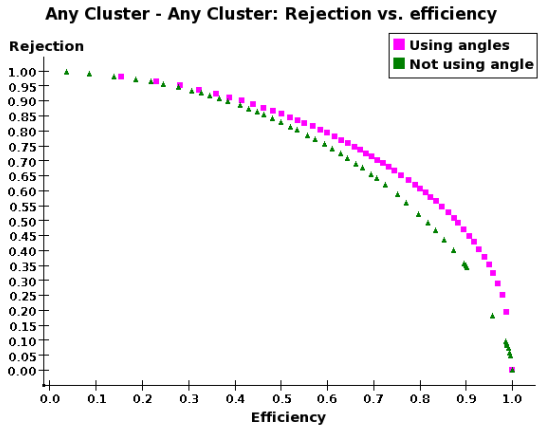

Figure 3: Rejection vs efficiency plot for any two sub-cluster pairs with and without the angles used in the likelihood$b$ and c.

Clearly steps 4 and 5 are totally intertwined; step 6 described next for shower building is a central piece of the algorithm and is the culmination of all of the pieces developed so far. It was planned as a two-step process.

6) Shower reconstruction: In the first pass we construct the shower skeleton with very high purity going outward (unidirectional) with resaonable efficiency with no optimization. The skeletons are constructed for all tracks starting from the track seeds. In the second iteration the skeletons of the track's showers are extended by adding other sub-clusters with proper arbitration among different tracks. In treating all tracks simultaneously we intend to avoid favoring any track. In the baseline each track's shower was fully reconstructed until the reconstructed energy (E) matched the track momentum (p), "stealing" shower pieces belonging to other, low-energy tracks. Now we also avoid E and p matching to be the biggest arbitrator and use this criterion judiciously.

4 Plans for Improvement

In Section three we described a plan for incremental progress in the existing Iowa PFA which was successfully executed. However, we also recognized that the underlying approach used in this PFA was now beginning to reach its limits. Therefore, in parallel, we bagen to develop a new, more general alogorithm. We outline this approach below. In the end the project was too amibitious to bear fruit within the time frame of this project, but the progress made and code written remain available.

Upon obtaining a reasonable resolution from the 3-D overall shower reconstruction. We started a different shower reconstruction philosophy where we follow the development of ecah shower starting with the innermost layer through each succesive layer. Any secondary shower starting as a fragment of the primary is also tracked the same way following its development layer-by-layer. MIPS are identified by the point-like hits and a typical energy deposit. Photons are expected to start in the ECAL, some are followed through into HCAL. Essentially, it is a following of the shower development through each layer hit-by-hit in the first pass-through. Charged hadrons are characterized by their MIP-like beginning and late development. Neutral hadrons are identified by their shower shapes and energy deposit over a few of the layers. A probability is assigned and

in a second iteration, the energy of each component of shower is matched. We wanted to develop this idea fully. We made quite a bit of progress with the SiD02 geometry in the barrel region, but clearly crossovers between boundaries needed details of the geometry, and this was not available with SiD02 as it stood. The associated software was frozen to establish the proof-of-principle result which we hoped to be of a comparable resolution with that of PANDORA. The late Ron Cassell was an expert at the infrastaructure and geometry; his expertise were, and still is, sorely missed. With no new funding and lack of infrestructure in connecting with realistic SiD geometry we were basically stymied.

PANDORA works very well. We wanted to establish an entirely independent algorithm and to cross-check the physics results obtained through PANDORA. In addition development of expertise in a PFA has a long learning curve which was accomplished by both Remi and Garabed. Nevertheless, we had to stop pursuing the effort any further.

5 Summary

We successfully carried out a program of improvements to the Iowa PFA, improving the resolution at 1 TeV from 6.3% to 5.5% and reducing the cpu time by more than a factor of two on average per event. We also began a more ambitious rewrite of the PFA, incorporating our experience and what the LC community has learned over the past decade. This latter was too big a project to complete with the limited resources available, but what we learned will form a good base for future efforts.